



LAWRENCE  
LIVERMORE  
NATIONAL  
LABORATORY

# Equivalent continuum modeling for shock wave propagation in jointed media

Oleg Vorobiev, Tarabay Antoun

December 16, 2009

## **Disclaimer**

---

This document was prepared as an account of work sponsored by an agency of the United States government. Neither the United States government nor Lawrence Livermore National Security, LLC, nor any of their employees makes any warranty, expressed or implied, or assumes any legal liability or responsibility for the accuracy, completeness, or usefulness of any information, apparatus, product, or process disclosed, or represents that its use would not infringe privately owned rights. Reference herein to any specific commercial product, process, or service by trade name, trademark, manufacturer, or otherwise does not necessarily constitute or imply its endorsement, recommendation, or favoring by the United States government or Lawrence Livermore National Security, LLC. The views and opinions of authors expressed herein do not necessarily state or reflect those of the United States government or Lawrence Livermore National Security, LLC, and shall not be used for advertising or product endorsement purposes.

This work performed under the auspices of the U.S. Department of Energy by Lawrence Livermore National Laboratory under Contract DE-AC52-07NA27344.

# Equivalent continuum modeling for shock wave propagation in jointed media

---

*Oleg Vorobiev and Tarabay Antoun*

Lawrence Livermore National Laboratory L-231, P.O. Box 808, Livermore, CA 94550, USA

## **Abstract**

This study presents discrete and continuum simulations of shock wave propagating through jointed media. The simulations were performed using the Lagrangian hydrocode GEODYN-L with joints treated explicitly using an advanced contact algorithm. We studied both isotropic and anisotropic joint representations. For an isotropically jointed geologic medium, our results show that the properties of the joints can be combined with the properties of the intact rock to develop an equivalent continuum model suitable for analyzing wave propagation through the jointed medium. For an anisotropically jointed geologic medium, we found it difficult to develop an equivalent continuum (EC) model that matches the response derived from mesoscopic simulation.

We also performed simulations of wave propagation through jointed media. Two approaches are suggested for modeling the rock mass. In one approach, joints are modeled explicitly in a Lagrangian framework with appropriate contact algorithms used to track motion along the interfaces. In the other approach, the effect of joints is taken into account using a constitutive model derived from mesoscopic simulations.

## INTRODUCTION

Equivalent Continuum (EC) methods present a viable approach for numerical simulations of heavily jointed or particulate medium such as jointed geologic formations, bolder fields, granular materials etc. Such methods operate in the frame of continuum mechanics where multiple discontinuities are accounted for implicitly using parameters which define mechanical properties of the materials. One example of such parameters is the Geologic Strength Index (GSI) frequently used in rock engineering to characterize the quality of rock masses.

Numerical simulation can help understand mechanical behavior of heavily jointed media and derive appropriate functional forms for material models used to describe such media. Analytical methods developed earlier for jointed rock masses [4, 5] can only be applied to small deformations and do not account for nonlinear irreversible processes taking place during large deformations.

There have been attempts to use both DEM and FE methods to determine the properties of the fractured rock mass [6, 8, 9, 13]. In the present work we are trying to develop a methodology to build Equivalent Continuum models for nonlinear wave propagation through heavily jointed rock media.

The model used in this study has been applied for numerical simulation of wave propagation in the intact rock samples [1, 15]. It includes parameters which characterize the quality of rock and can be also applied to jointed rock mass. Since most of model parameters are derived from the experimental data for small intact rock samples the scaling of these parameters to large size rock masses is very important. In the absence of reliable large scale testing for the jointed rock, numerical modeling can help understand how the response of the rock masses differs from the small samples and to establish the scaling rules if they exist.

## SIMULATIONS OF NONLINEAR WAVE PROPAGATIONS IN JOINTED ROCK

### Material model for intact rock samples

Because of their heterogeneous nature rock materials exhibit complicated mechanical behavior. They are brittle at low confinements and ductile at high pressures. To model this behavior advanced plasticity models describing porous compaction and dilation, softening and hardening, rate and scale dependence have been developed. Such models can be calibrated by comparing results of triaxial loading of a single material point with the experiments. The model used in the current study operates in the frames of isotropic plasticity theory and was described in detail in [1]. Therefore, here we will describe only the yield surface used in the model.

The ultimate strength function,  $Y_f(p)$ , is based on the Hoek-Brown strength criterion [2] that relates the maximum ( $\sigma_1$ ) and minimum ( $\sigma_3$ ) principal stress on the failure surface as

$$\sigma_1 = \sigma_3 + Y_c \left( m \frac{\sigma_3}{Y_c} + s \right)^n \quad (1)$$

For most rocks  $\frac{1}{2}$  is a reasonable value for  $n$ . The parameter  $s$  is equal to unity for intact material and less than unity for in situ material. Hoek-Brown model gives an empirical relationship between the coefficients  $s$  and  $m$  and the Geologic Strength Index (GSI)

$$s = \exp\left(\frac{GSI - 100}{9}\right), m = m_i \exp\left(\frac{GSI - 100}{28}\right) \quad (2)$$

In Eq. (2),  $m_i$  is the value of  $m$  for intact rock; it can be obtained from static lab tests. For triaxial compression with  $\sigma_e = Y_f$ , the principal stresses  $\sigma_1$  and  $\sigma_3$  are given by

$$\sigma_1 - \sigma_3 = Y_f, \quad \sigma_3 = p - \frac{Y_f}{3}, \quad (3)$$

so that the H&B function (1) yields

$$\frac{Y_f}{Y_c} = \left( s + \frac{mp}{Y_c} - \frac{mY_f}{3Y_c} \right)^n \quad (4)$$

When  $n=0.5$ , Eq. (4) becomes a quadratic equation and the failure strength,  $Y_f$ , can be expressed in terms of pressure and unconfined compressive strength,  $Y_c$ , as

$$Y_f = Y_c \left[ \sqrt{s + \frac{m^2}{36} + \frac{mp}{Y_c}} - \frac{m}{6} \right] \quad (5)$$

Eq. (5) may not be flexible enough to describe uniaxial strength both in compression and tension. Therefore the following, more general function is used

$$Y_f(p) = \begin{cases} Y_{f1}(p) & p > Y_c/3 \\ Y_{f2}(p) & p \leq Y_c/3 \end{cases}, \quad (6)$$

where the functions  $Y_{f1}$  and  $Y_{f2}$  are expressed as

$$Y_{f1}(p) = Y_c \left[ \left( s + \frac{m^2}{36} + \frac{mp}{Y_c} \right)^n + s^n - \left( s + \frac{m^2}{36} + \frac{m}{3} \right)^n \right], \quad (7)$$

$$Y_{f2}(p) = \frac{\langle p/Y_c + s\beta \rangle}{1/3 + \beta}, \quad \beta = \frac{2R_t}{3(1 - R_t)}, \quad R_t = Y_t/Y_c \quad (8)$$

The value of  $Y_c$  for intact material can be found from unconfined compressive tests. Both  $Y_c$  and  $Y_t$  can be parametrized in terms of the reference porosity  $\Phi$  as was done in [9].

Figure 1 shows the yield surface evolution in the Y-P plane. The ultimate yield surface is achieved in the limit of high plastic strain as a result of the strain hardening. The material behaves elastically until it reaches the cap surface. Then it accumulates plastic strain during porous compaction following the path between the initial cap surface and the ultimate yield surface.

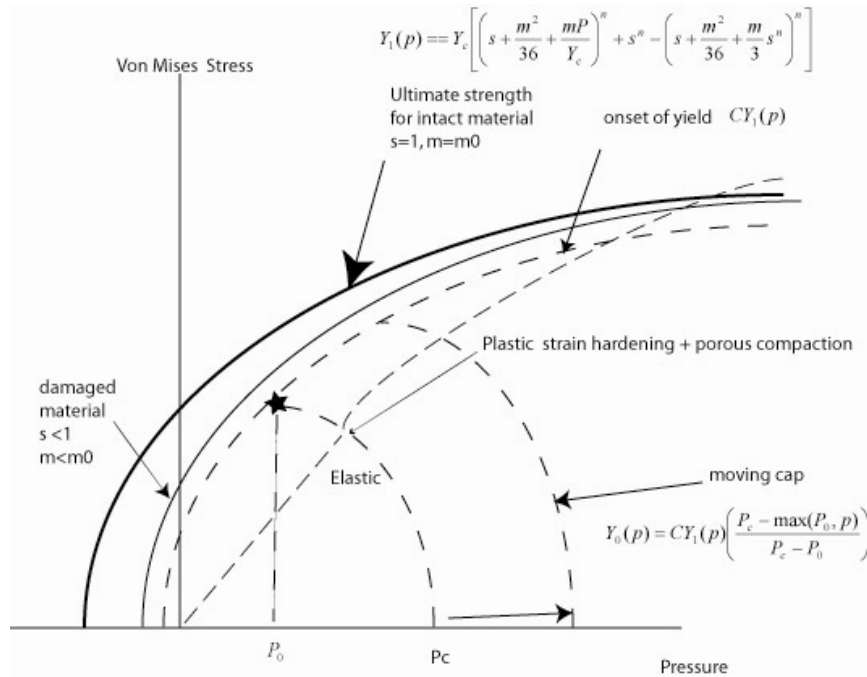


Figure 1A. Yield surface in Y-P plane. The cap separating elastic and plastic regions on the right moves with compaction. The pressure corresponding to the beginning of compaction in hydrostatic conditions  $P_c$  is defined by the compaction curve (Fig.1B). Uniaxial strain loading path is shown with the bold dashed line.

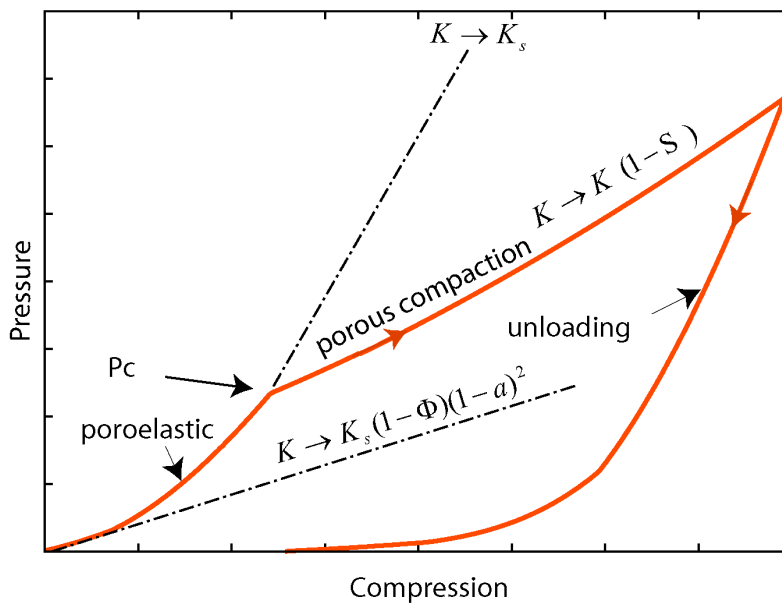


Figure 1B. Pressure evolution in loading-unloading cycle

The model describes nonlinear elasticity (poroelasticity) observed in porous rocks as shown in Fig. 1B.

Thus the initial bulk modulus can be adjusted by varying the poroelasticity coefficient  $\alpha$ . The effective bulk modulus,  $K$ , is further modified by the compaction slope,  $S$  at the onset of the porous compaction.

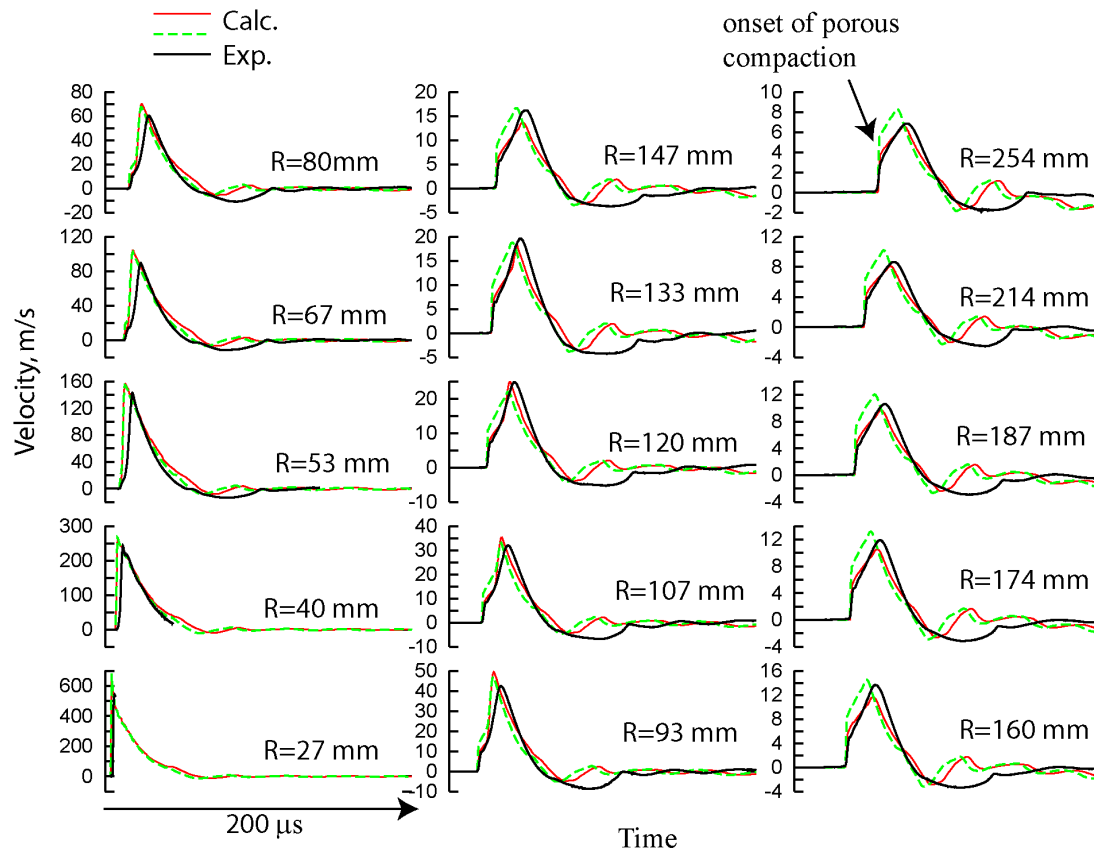


Figure 2. Comparison of experimental (bold lines) and simulated radial velocity at different ranges induced in 12 % porous limestone by a spherical explosion. The dashed lines correspond to an increased value of  $P_c$ .

The material model built to reproduce mechanical response measured in Salem Limestone in triaxial tests was extended further to describe the wave generation and propagation in dynamic experiments [14]. Figure 2 shows the radial velocities histories measured at different ranges from the source together with our calculated results. In previous studies [15] we identified the main model parameters controlling the shape of the pulse. The first one is the compaction pressure,  $P_c$ , at which the pores in the material begin to collapse irreversibly. The onset of porous compaction can be seen in the measured and the calculated velocity histories shown in Fig 2. In hydrostatic compaction tests this phenomenon can be seen as a change of slope in the pressure-volume path. Also, it was shown that the porous dilation (bulking) may be very important, especially in divergent flows [15]. The current model includes both compaction and dilating as described in [1].

## Joint model

It is known from experimental observations that joint normal closure is a non-linear function of applied normal stress, resembling a hyperbola [3]. Therefore the normal modulus of a joint,  $E_j$ , can be expressed as

$$E_j = E_{j0} \frac{a^2}{(a - u_{max})^2}, \quad (9)$$

where  $u_{max}$  is the maximum joint closure for all times. According to Eq.(9), the normal force is very nonlinear in loading and linear in unloading as shown in Fig.3.

The normal force  $F_n$  and the shear force  $F_s$  are incremented proportionally to the respective moduli  $E_j$  and  $G_j$  as

$$\Delta F_n = A_c E_j \Delta_n / a \quad \Delta F_s = A_c G_j \Delta_s / a, \quad (10)$$

where  $A_c$  is the area of contact and  $\Delta_n, \Delta_s$  are the normal and the shear displacement increments. The shear forces are limited by the yield surface dependent on the normal force as

$$F_{smax} = \sigma_{coh} A_c + F_n \mu, \quad (11)$$

where  $\sigma_{coh}$  is the shear cohesion and  $\mu$  is the friction coefficient related to the friction angle as  $\mu = \tan(\varphi)$ .

Anytime the yield surface is applied to restrict the shear force, the shear slip,  $u_{sp}$ , is accumulated as

$$\Delta u_{sp} = \frac{\langle |F_s| - F_{smax} \rangle}{G_j A_c} \quad (12)$$

The friction coefficient changes with the amount of shear slip to account for softening effects as

$$\mu = \mu_r + (\mu_0 - \mu_r) \left(1 - \frac{u_{sp}}{u_{sp0}}\right), \quad (13)$$

where  $\mu_0$  and  $\mu_r$  are the initial and the residual friction angles, and  $u_{sp0}$  is the critical shear slip. Figure 3 shows schematically the transition from the slope  $\mu_0$  to the slope  $\mu_r$  during the shear slip.

To account for joint dilation due to shear slip, the normal forces can be adjusted anytime the shear slip is incremented as

$$\Delta F_n = A_c E_j \left\langle 1 - \frac{F_n}{F_{crit}} \right\rangle \tan(\Psi) \Delta u_{sp}, \quad (14)$$

where  $\Psi$  is the dilation angle and  $F_{crit}$  is the critical normal force above which dilation will not occur. The details of the numerical implementation are described in [11].

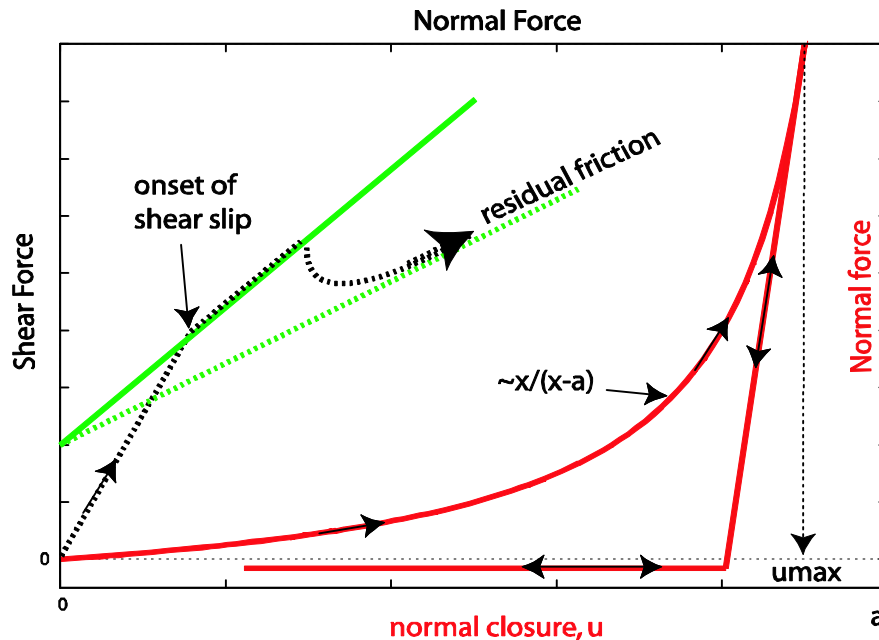


Figure 3. Schematic plot for the dependence of the shear force vs normal closure (one the left) and the normal force vs normal closure at the joint.

The functional form used by Eq.(9) for the joint stiffness was chosen based on empirical data for quasi-static joint tests. To validate the model for a dynamic case, two sets of spherical wave experiments [14] performed at SRI with Salem limestone were simulated (one with a joint and the other one without). Radial velocity (along the joint surface) at various ranges was measured in these experiments as shown in Fig.4.I. The spherical charge consisted of 3/8 g of PETN explosive initiated at its center. A single joint placed 2.6 cm away from the charge was studied. Two computational domains interacting through a contact boundary were used in 2D axisymmetric calculations shown in Fig.4.II. No softening and a zero cohesion were assumed in the calculations. The joint aperture size of 0.1 mm was used. Parametric study showed a weak effect of the aperture size on the calculation results. Figure 5 shows comparison of the experimental records (on the right) with calculations performed using four different friction angles at the contact. Experiments show that, at range 2.79 cm, all three velocities (the incident, the transmitted and the free-field velocity) are close until the sliding on the joint is activated. Calculations reveal that the onset of sliding (shown with a square in fig. 5) is mainly controlled by the joint friction. Thus, by increasing the friction angle the sliding can be delayed. Also, the smaller the friction angle, the larger the difference between the transmitted and the incident velocities. Experimentally measured free field velocities (without the joint) at the same ranges are shown with bold dotted lines.

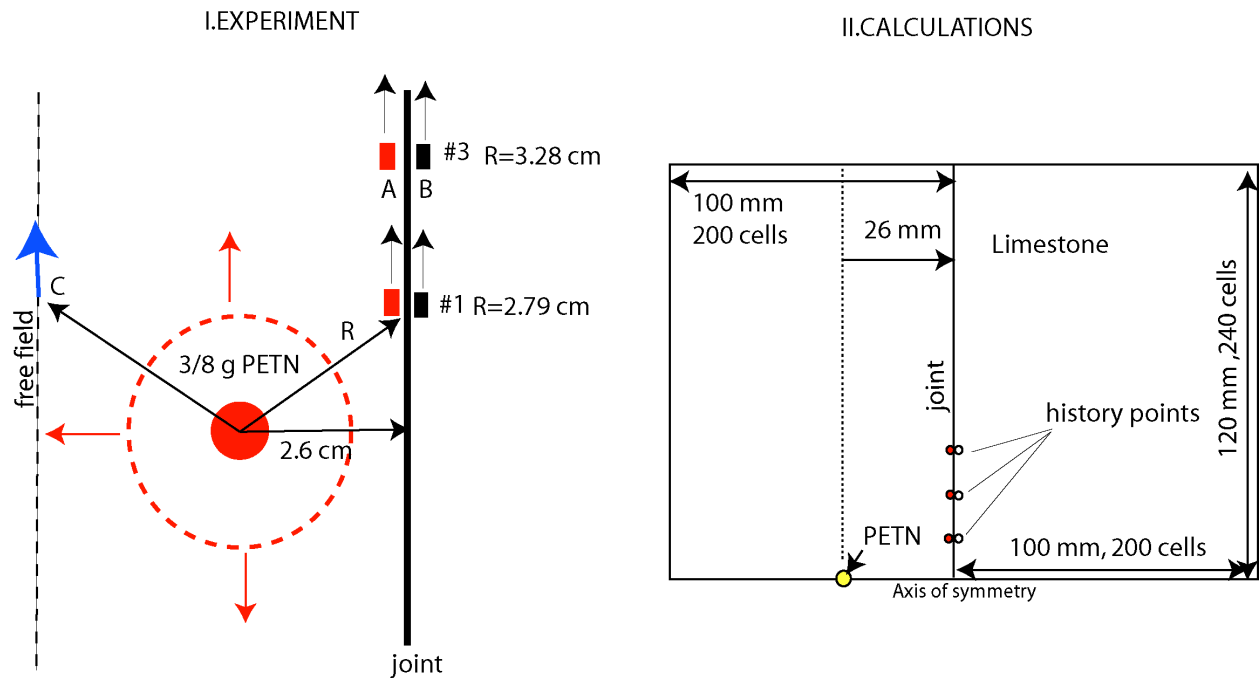


Figure 4. Experiment set-up (I) and calculation set-up (II). Radial velocities were measured before the joint (location A), after the joint (location B) and at the same range in the free field (location C)

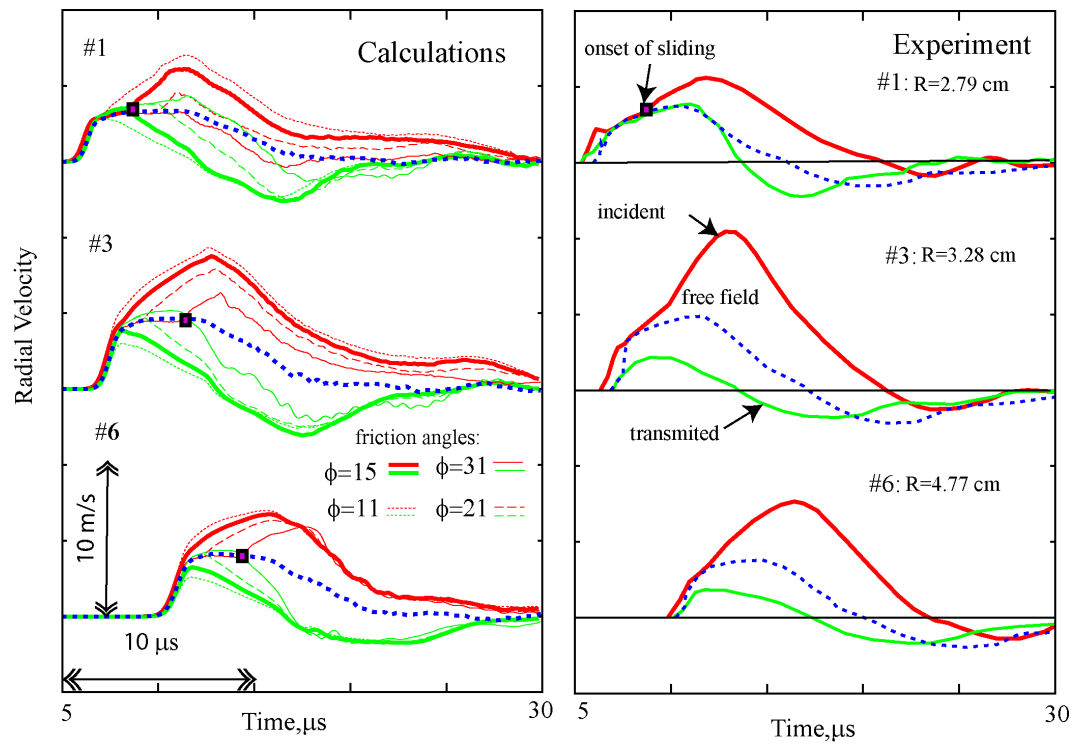


Figure 5. Measured and calculated radial velocity histories at three different ranges ( $R=2.79$  cm,  $R=3.28$  cm and  $R=4.77$  cm). Calculations were performed for four different friction angles.

## Numerical method

The explicit finite-difference code GEODYN-L [9,11] was used to update the elements. The joints between the elements were modeled using the Simple Common Plane contact algorithm described in [11].

## Study of mechanical response for jointed media

The spacial distribution of joints has an effect on the wave propagation. Figure 6 shows the problem setup for the calculations of 2D cylindrical waves in a jointed medium with two sets of joints, with the same joint spacing in each direction. The joints were fully persistent in the X-direction and semi-persistent in the other direction. Thus, the square blocks cut by the joints were staggered in the Y-direction as shown in Figure 6. Each block was subdiscretized into quad elements and the contacts were set at the external faces of these elements. The symmetry planes were set along the X and Y axes. The energy was instantly deposited within a radius of 20 mm from the point (0,0). Two different specific energies of 5 kJ/g and 50 kJ/g were considered. An energy-dependent Mie-Grueneisen EOS was used for the limestone, described in detail in [1]. The deposited energy generated a thermal pressure in the material propagating outwards into the jointed region as a cylindrical shock wave. Figures 7- 8 show the contours of pressure and plastic strain for calculations with different joint spacing at a time of 100 microseconds. Increased joint density enhances the anisotropy of the medium. This is especially seen in the plastic strain contours for the low specific energy shown in Fig. 8B, where the damage is localized mainly in the X- and Y directions. Also, it is noticeable on the pressure contours (Fig. 7A-8A) that the wave propagates slower as the joint density increases. For high specific energy the wave generated is strong enough to lock the joints so that the material response resembles that of the continuum, as is seen from the pressure contour plot shown in Fig 7A. The differences increase when the pressure drops. Also, due to the difference in the normal stiffness, the elastic wave propagates slower in the jointed medium. More information on the study on cylindrical wave propagation through a jointed medium with two sets of joints can be found in [10].

It is evident from this study that the equivalent continuum model for a medium with two sets of joints should be based on an anisotropic plasticity model. We used an isotropic plasticity model, which could only be applied if the joints were distributed randomly. Therefore we will focus more on media with randomly distributed joints. The method used previously in [9] for quasi-static loading of randomly jointed rock was used in this study to create such a distribution, where the existing unstructured mesh was separated into blocks of elements grouped by proximity to randomly seeded centers of spheres with all elements centered within the sphere belonging to the same group. Figure 9 shows the hoop stress calculated for a cylindrical wave propagating through the randomly jointed medium. The cases A,B,C,D corresponding to different joint densities; all produce symmetric cylindrical flow. Since the joints initially are more compressible than the rock, the presence of the joints has an effect on the wave propagation speed, as can be seen from the picture.

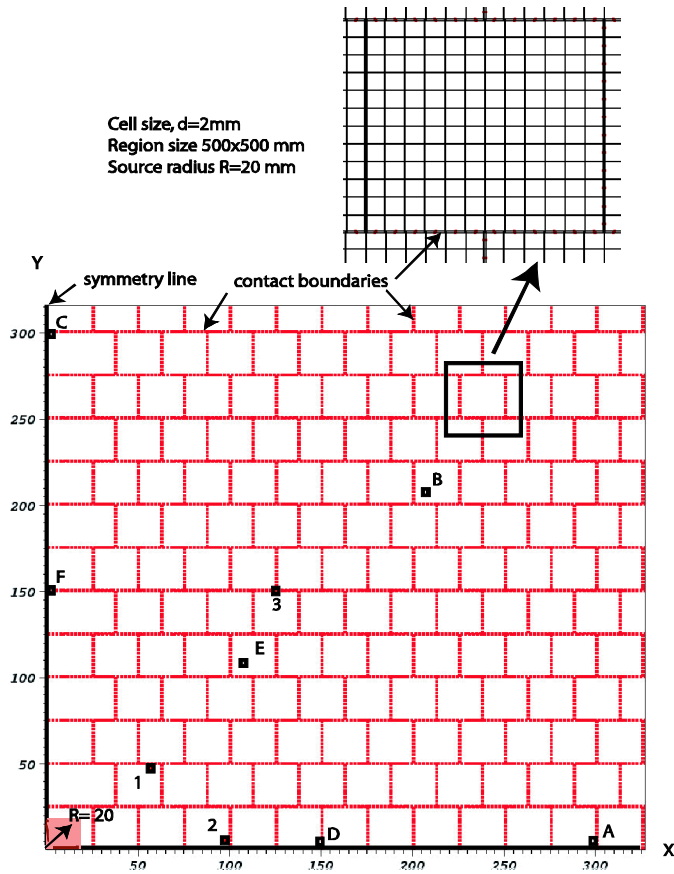


Figure. 6 Problem set-up for cylindrical wave propagation through two sets of joints

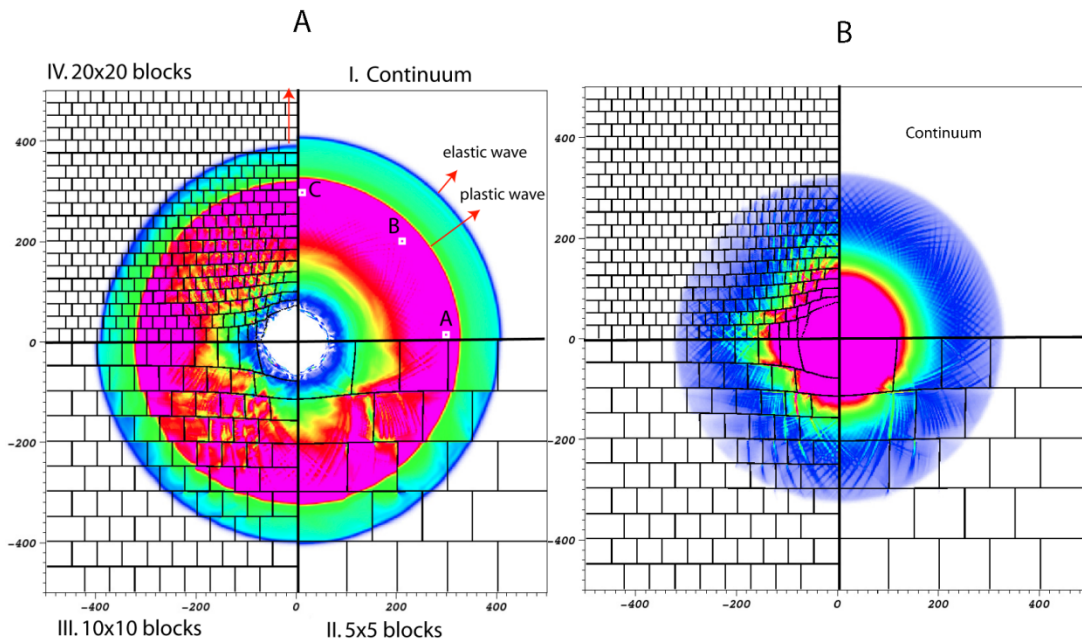


Figure 7. Pressure (A) and plastic strain (B) contours at time  $100\ \mu\text{s}$  for different joint densities. The pressure range is 0-0.2 GPa and the strain range is 0-0.1. The specific energy for the source is 50 kJ/g and the friction angle used for the joints is 21 degree.

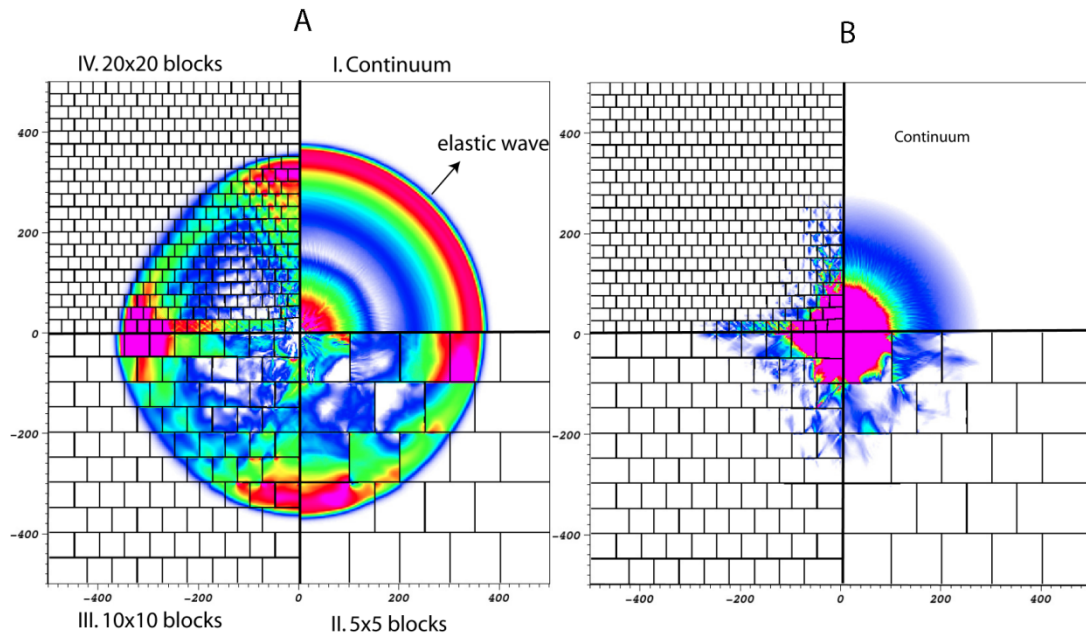


Figure 8. Pressure (A) and plastic strain (B) contours at time  $100 \mu\text{s}$  for different joint densities. The pressure range is 0-0.05 GPa and the strain range is 0-0.01. The specific energy for the source is 5 kJ/g and the friction angle used for the joints is 11 degree.

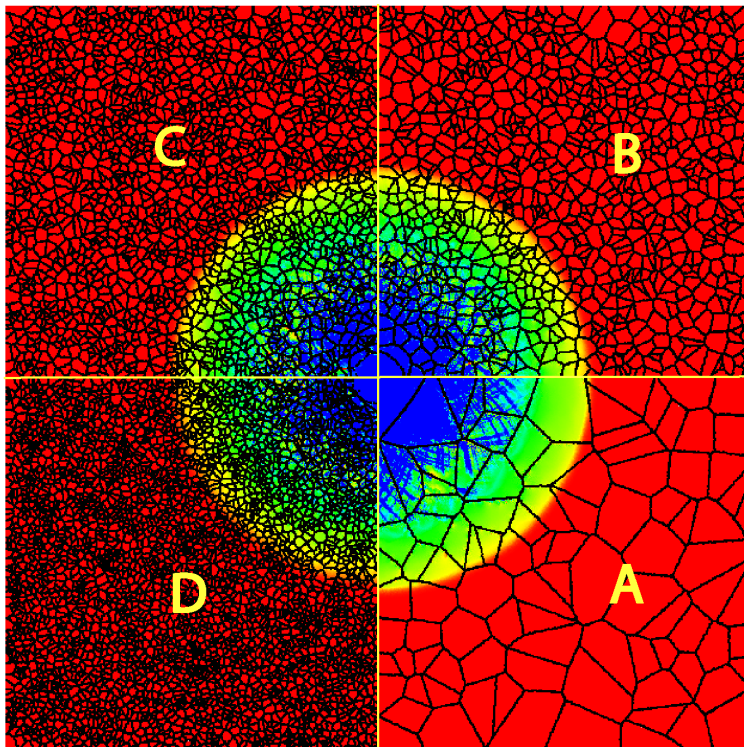


Figure 9. Hoop stress contours at time  $160 \mu\text{s}$  for four discrete media with different number of randomly distributed blocks: A-100 blocks, B-1000 blocks, C-2000 blocks, D=4000 blocks

## Representative volumes and average response

Figure 10 shows locations of the representative volumes in the problem of cylindrical wave propagation in an infinite randomly jointed medium. The energy was instantly deposited in a spherical region as shown in the figure. The Representative Volumes (RVs) were defined as a union of all elements centered within the given distance from the volume center. Two sizes of RVs of 50 mm (small) and 100 mm (large) were used in a rectangular region with dimensions 1000X1000 mm.

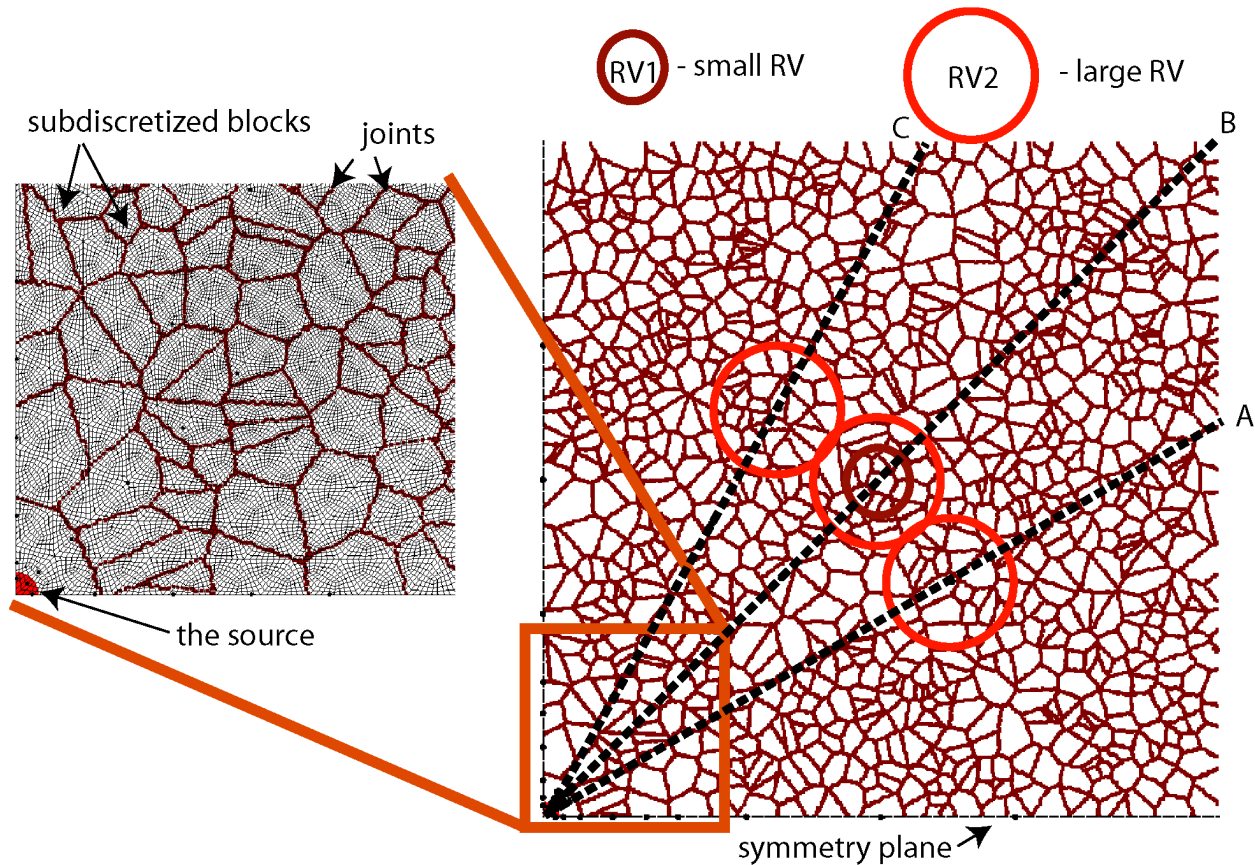


Figure 10. Block geometry and RV point locations for the jointed medium with 1000 blocks

The stress state for the volume was found and the volume-averaged stress. The average velocity for different RVs is plotted in Fig.11 at two locations ( $R=200$  mm and  $R=700$  mm) in B direction for various random realization of 1000 block assembly. It is seen from the picture that the peak velocity varies significantly for different realizations when the value for the velocity is taken from the nearest node to that location (low curves). Therefore, to ensure statistically meaningful correlations between the flow parameters, the size of RV should be big enough to represent the homogenized medium response. On the other hand, the bigger the RV the more smearing of the flow detail takes place. Thus, flow details smaller than the RV size cannot be captured. Figure 12 shows the effect of joint density on the velocity profile. Increasing the number of joints causes widening of the pulse and also affects the arrival time visible at longer ranges. Figure 13 shows the effect of friction angle on the wave form. For each friction angle radial velocity evolutions in all representative volumes are plotted to show that the friction effect is larger than the deviations between the different points located at the same range but in three different directions (A,B and C). It is also noticeable that these deviations are smaller when the friction angle of 31 is used compared to the friction angle of 11.

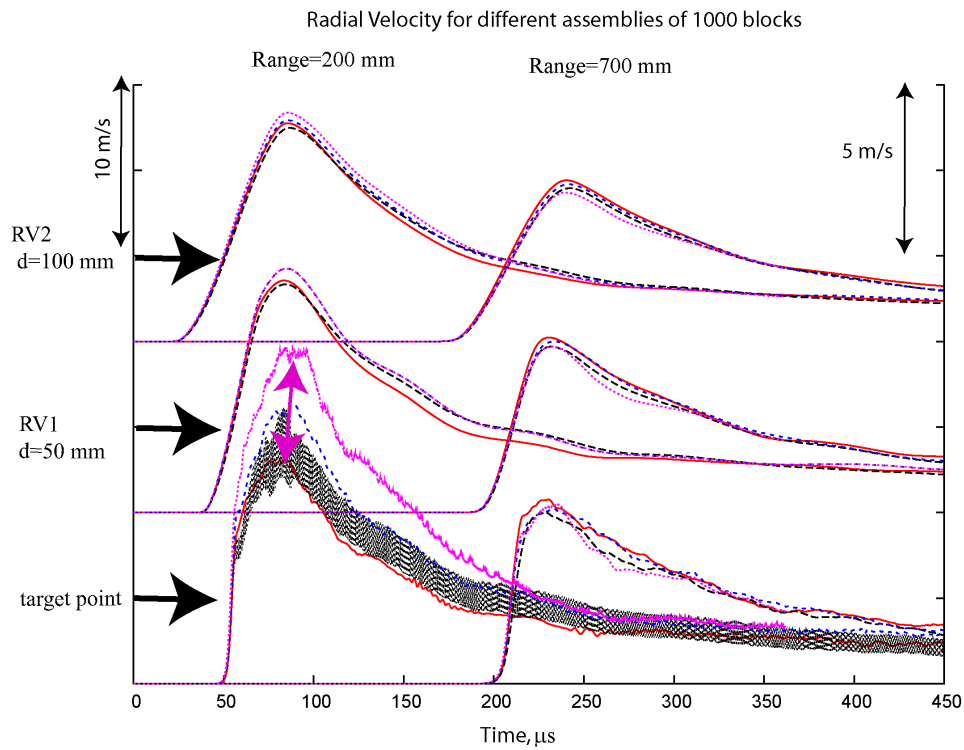


Figure 11. Averaged Radial velocity evolutions in RV elements of two different sizes (RV1 and RV2) for different random realization of the jointed medium with 1000 blocks

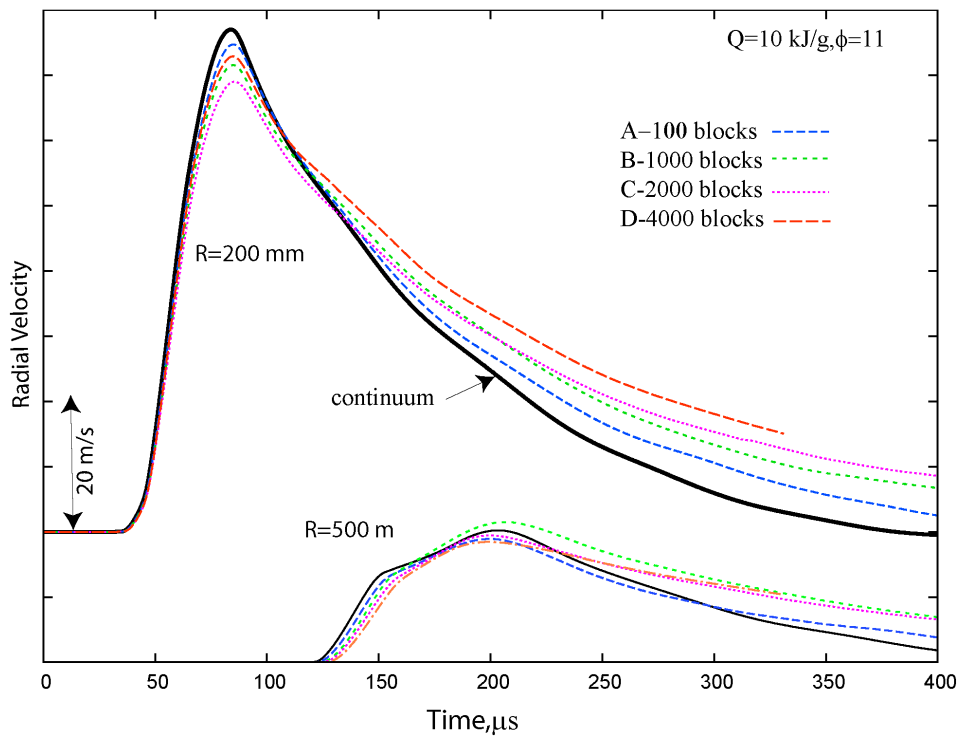


Figure 12. Radial velocity evolution for media with different number of discrete blocks

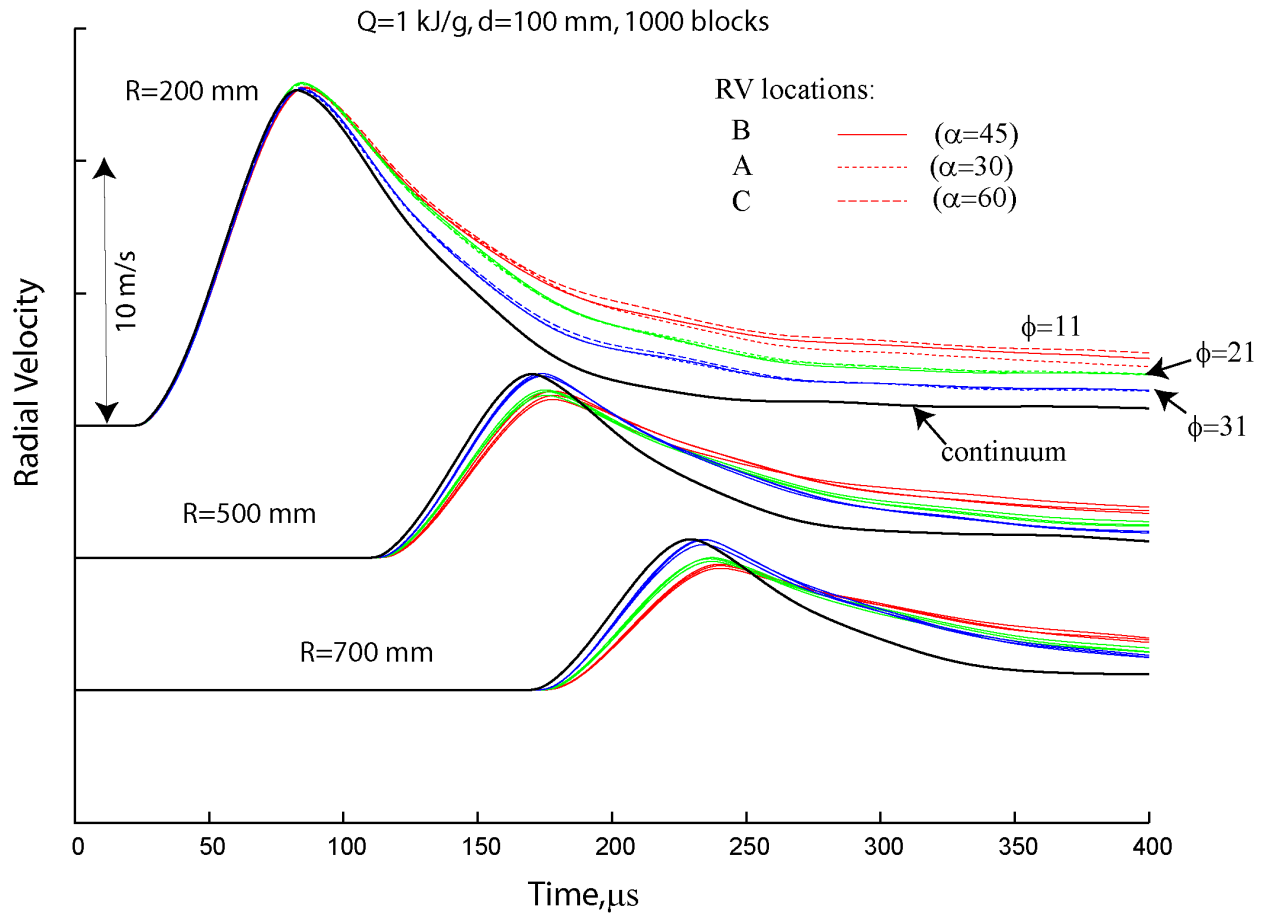


Figure 13. Effect of friction angle on the average radial velocity evolution for 1000-block-assembly at three different ranges

The calculated velocity profiles show that the flow can be considered isotropic and, therefore can be modeled by an equivalent continuum model. The simplest scaling built into the model is GSI-based scaling of the yield surface. We attempted to find the best GSI index so that the result of simulations with that EC model would match the discrete simulations. Figure 14 shows radial velocity evolution at two ranges plotted versus continuum simulation results obtained using different values of GSI shown with dashed lines. It is seen that Hoek-Brown scaling does not reproduce the high residual velocity and tends to overestimate the peak velocity. When only one of the parameters (parameter  $s$ ) was scaled according to the Hoek-Brown rule, the result was better but still not very good. Also, at a range 500 mm, the discrete simulations have a late arrival time compared to the continuum simulations. This is an indication that scaling just the yield surface the way it is done in rock engineering will not necessarily produce a good equivalent continuum model for nonlinear wave propagations.

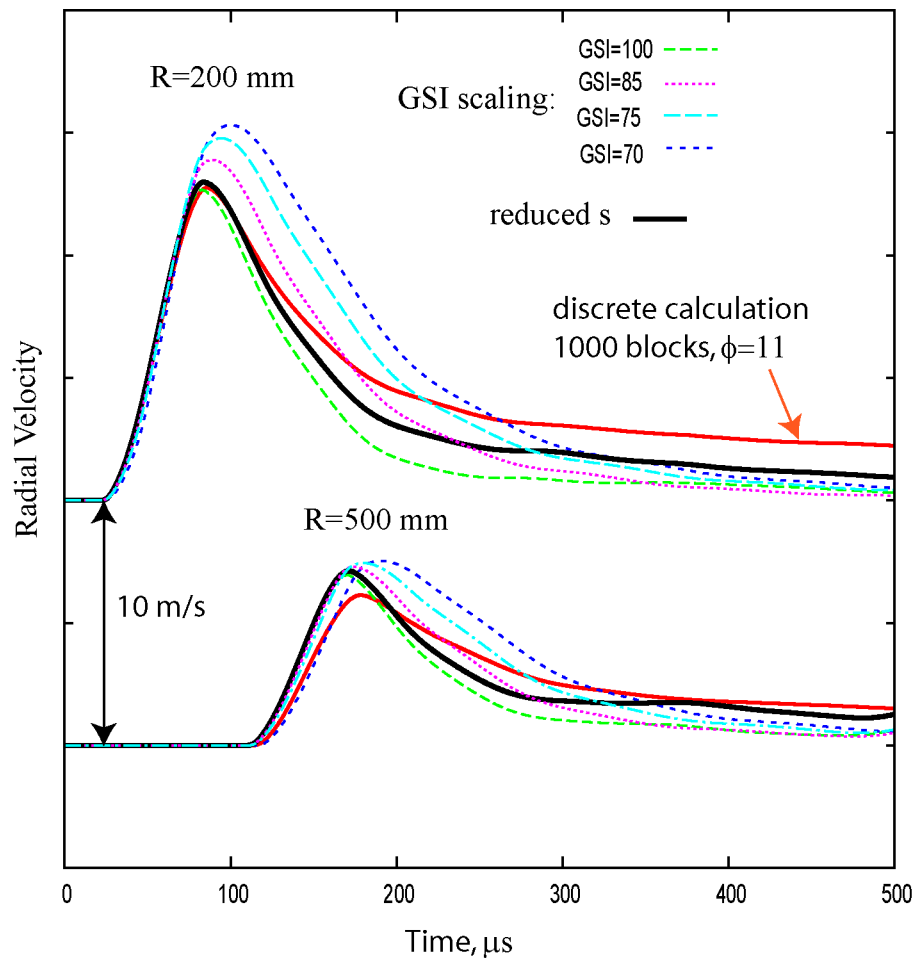


Figure 14. Comparison of the discrete calculation for the assemble of 1000 blocks (red solid line) with equivalent continuum calculations using different GSI index to scale the model.

## METHODOLOGY OF BUILDING HOMOGENIZED CONTINUUM FOR JOINTED ROCK MASSES

### Quasi-Static uniaxial loading

This method applies a uniform deformation for a representative volume (in this case the whole region) containing joints. Figure 15 shows a region with 1000 blocks subjected to a uniaxial compression. The initial velocities are chosen to provide a given velocity gradient. In addition to that, consistent set of boundary conditions is applied to maintain the given velocity gradient. Figure 16A shows axial stress vs axial strain for the whole region found in these calculations. When the joints were stiff ( $E=500\text{ GPa}$ ) the material response was the same as for the intact material. Reducing the initial joint stiffness changed mainly the initial elastic slope with the compaction slope remaining very close to one in the intact material. Figure 16B shows the compaction curve in pressure-volumetric strain coordinates calculated both for the intact materials (no joints) and for randomly jointed material with two joint densities ( $n=1000$  and  $n=2000$ ). Figure 17A shows the loading path in deviator-pressure space calculated for the jointed material ( $n=1000$ ) for three different friction angles. It is interesting to note that increasing the friction between the blocks causes high pressures to be generated at the same level of deviatoric stress.

This is due to an increased bulking on the block level generated due to low mobility of the blocks when high friction prevents them from sliding and closing the gaps. We have built two equivalent models scaling both the yield surface using the GSI rule described by Eq.(2) and modifying stiffness either by enhancing poro-elasticity (model #2) or by introducing a secondary porosity associated with the joints and an additional compaction of this porosity (model #1). The loading paths for uniaxial load-unload cycle for these two models is shown in Fig.17A with dotted lines.

Figure 17B shows that the friction between the blocks has even greater effect on the stress deviator than the joint density. As far as defining the effective stiffness the friction has a secondary effect compared to the joint density and joint stiffness. This is illustrated in Fig. 17C where the region of the strong joint effect is shown with a rectangle. Again, at high confinements, when the joints are locked effect of joints becomes less significant.

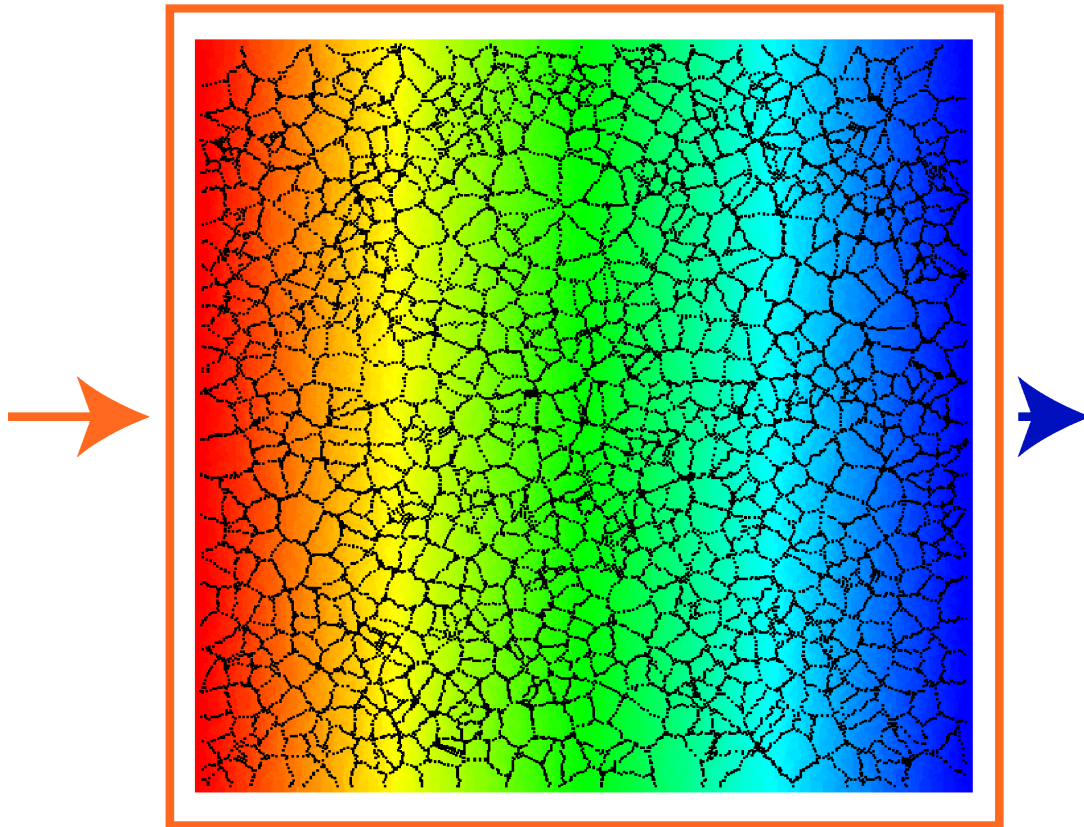


Figure 15. Initial velocity distribution and boundary conditions for quasi-static uniaxial loading of 1000 blocks.

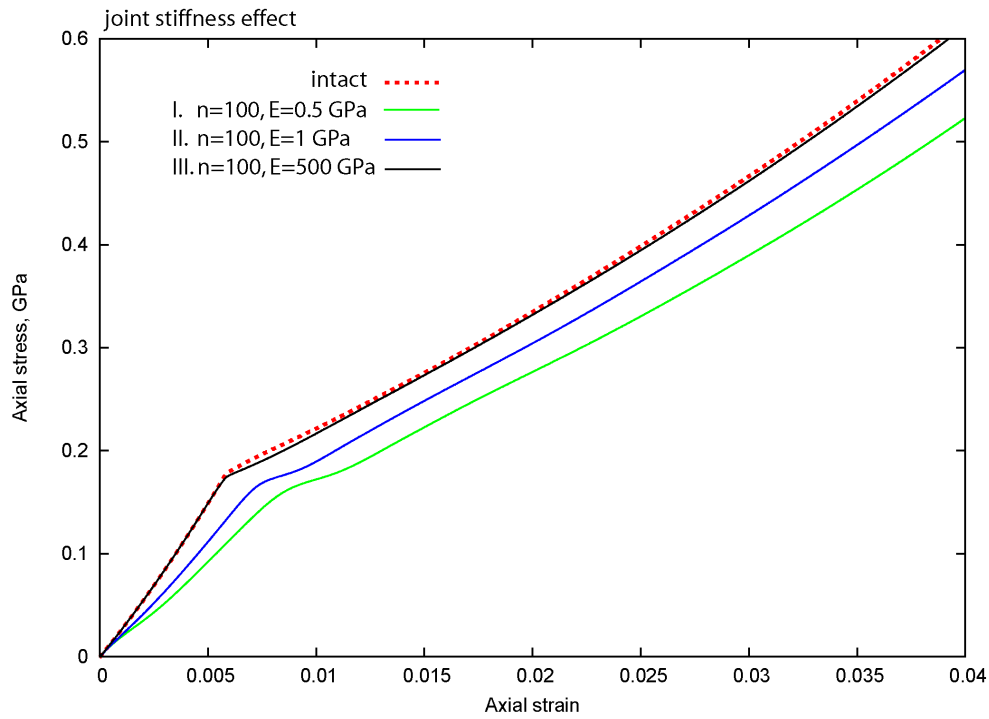


Figure 16A. Axial stress vs axial strain for quasi-static uniaxial loading of 100 blocks for various contact stiffness between the blocks.

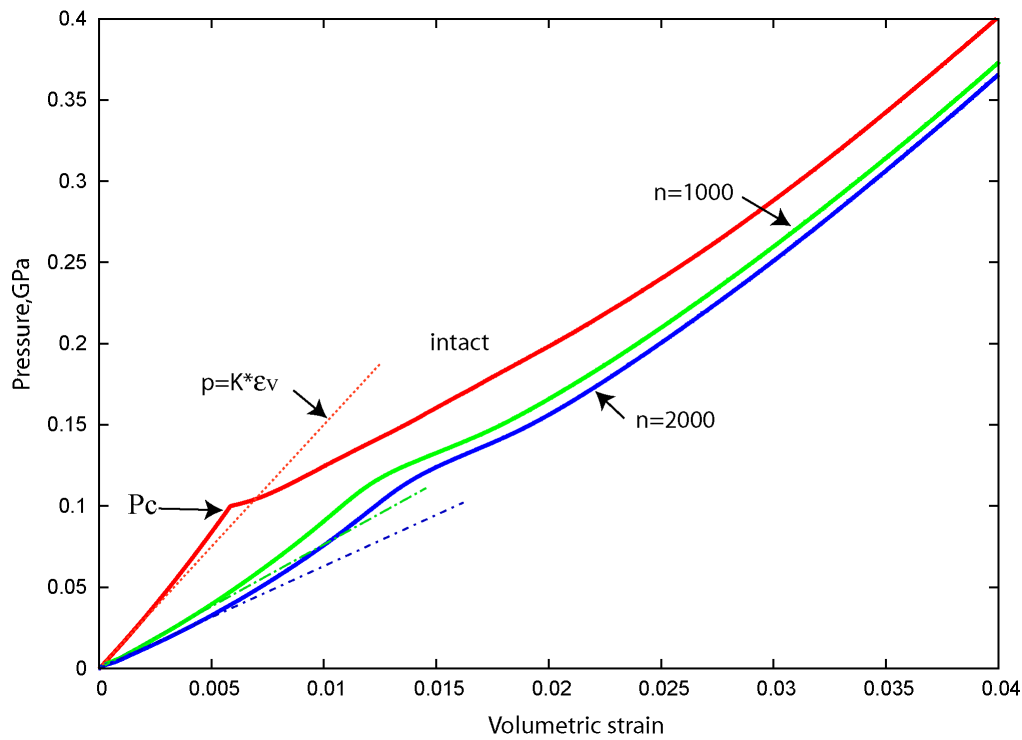


Figure 16B. Pressure vs volumetric strain in for quasi-static uniaxial loading for two different numbers of blocks ( $n=1000$  and  $n=2000$ ). The dotted lines show initial bulk modulus calculated using analytic expressions.

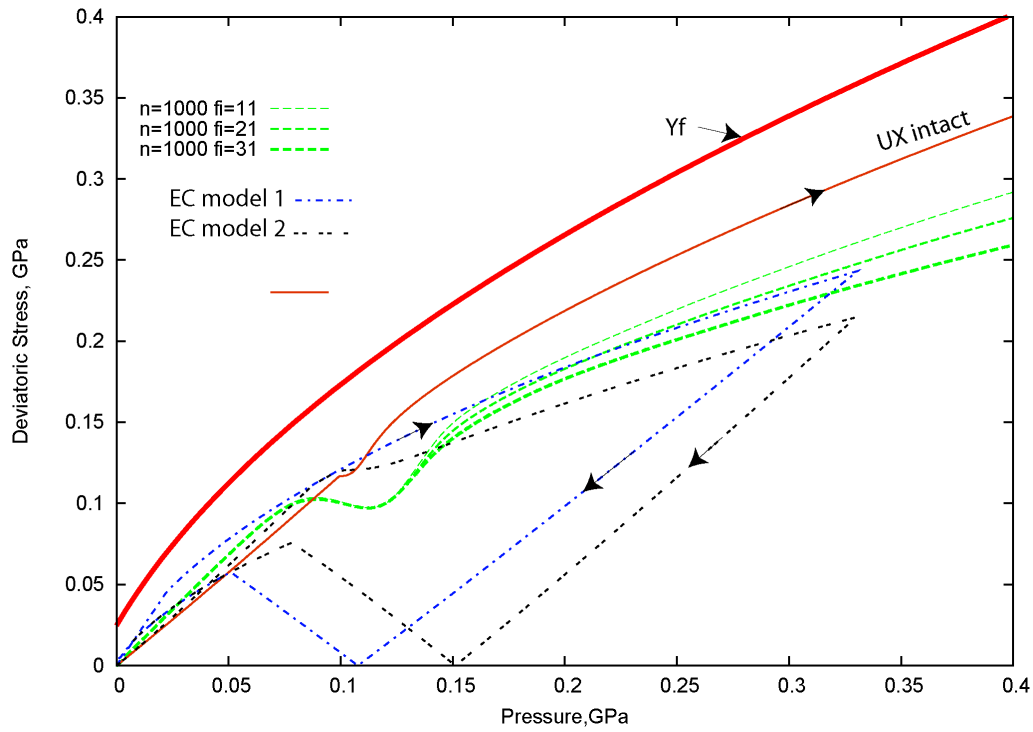


Figure 17A. Loading path in Y-p plane calculated for jointed media with 1000 blocks. The path for the intact material is shown with thin solid line and the paths for the equivalent models (model 1 and model 2) are shown with dotted lines.

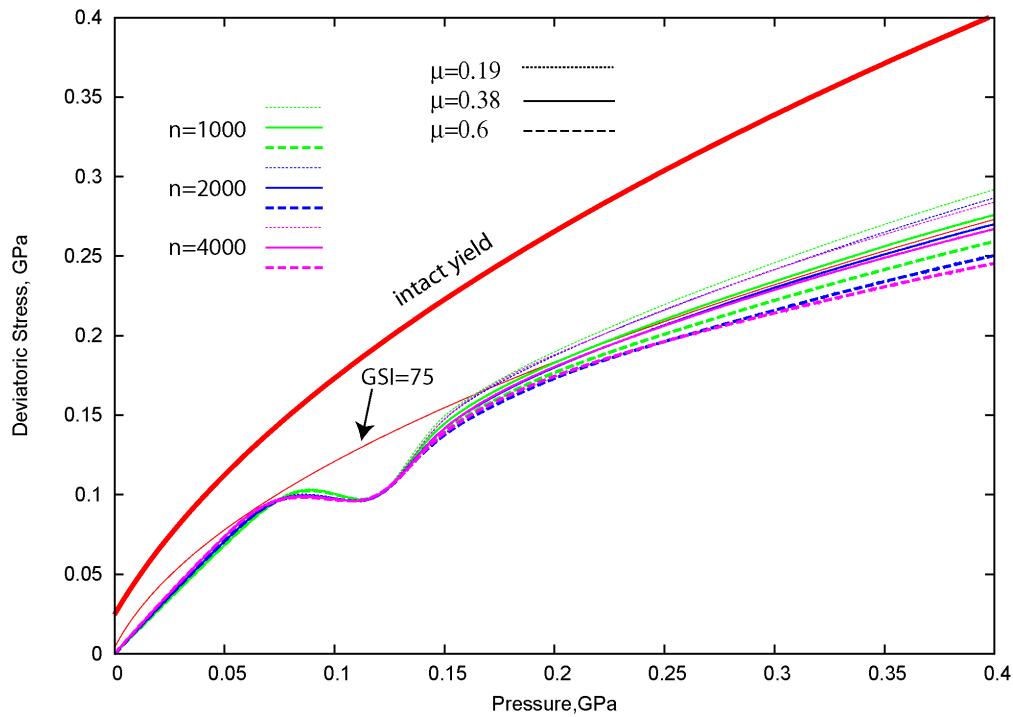


Figure 17B. Loading paths in Y-p plane calculated for jointed media with various number of blocks and three values of friction coefficient (0.19,0.38, 0.6)..

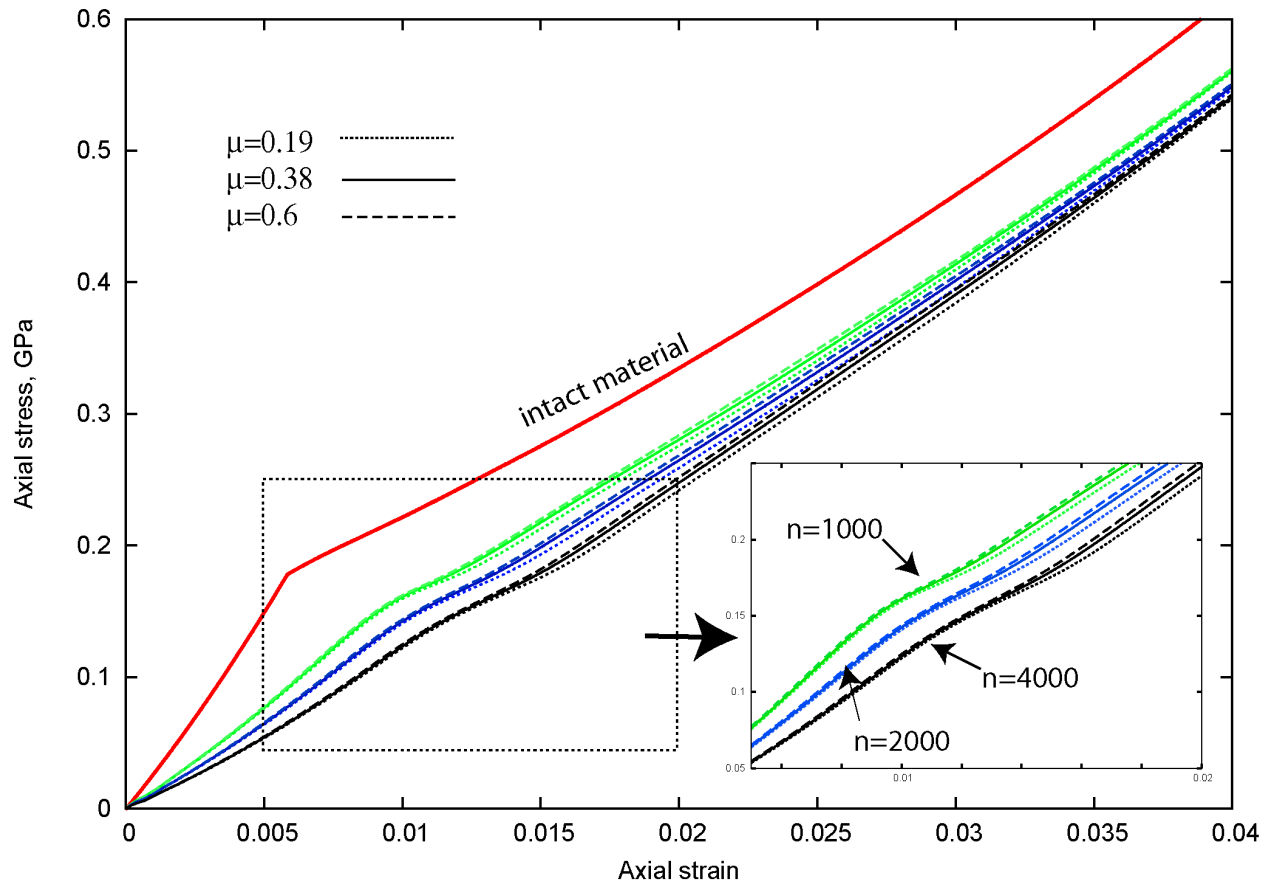


Figure 17C. Loading paths in stress-strain plane calculated for jointed media with various number of blocks and three values of friction coefficient (0.19,0.38, 0.6).

## Dynamic uniaxial loading

Figure 18 shows the problem set-up for the dynamic uniaxial loading of the jointed region. Constant x-velocity was applied at the left boundary and zero Y-velocity constraint was applied at the top and bottom boundaries. For a medium without joint this would result in 1D motion corresponding to a plane wave traveling from left to right. When the joint are introduced the motion is not strictly 1D because of multiple wave reflection from the joints which travel in Y direction. When the joint are randomly oriented the average motion may resemble one for a continuum with modified properties. The representative volumes (shown in Fig.18 with red circles) had a radius of 500 mm, the same as in the previous study with cylindrical wave propagation. It is seen from the picture, that for 100 blocks the RVs are not big enough to include statistically isotropic joint distribution, therefore the responses recorded in those volumes have significant variations. As it was shown in the previous study, bigger RVs could be used to reduce the variations but it will result in smearing the flow features such as, for example, elastic precursor. For 1000 blocks the same volumes produce noticeably smaller variations because they include much more joints with various orientations and, hence are more “representative” for the media with randomly oriented joints. Both cases (100 blocks and 1000 blocks) show an effect of deviatoric stress relaxation behind the plastic front, which could not be reproduced using continuum models without relaxation. Results for continuum simulations with weakened strength properties (GSI=75 and

GSI=85) are shown with dashed lines. The stress deviator is smaller but it stays constant behind the plastic front throughout the calculations.

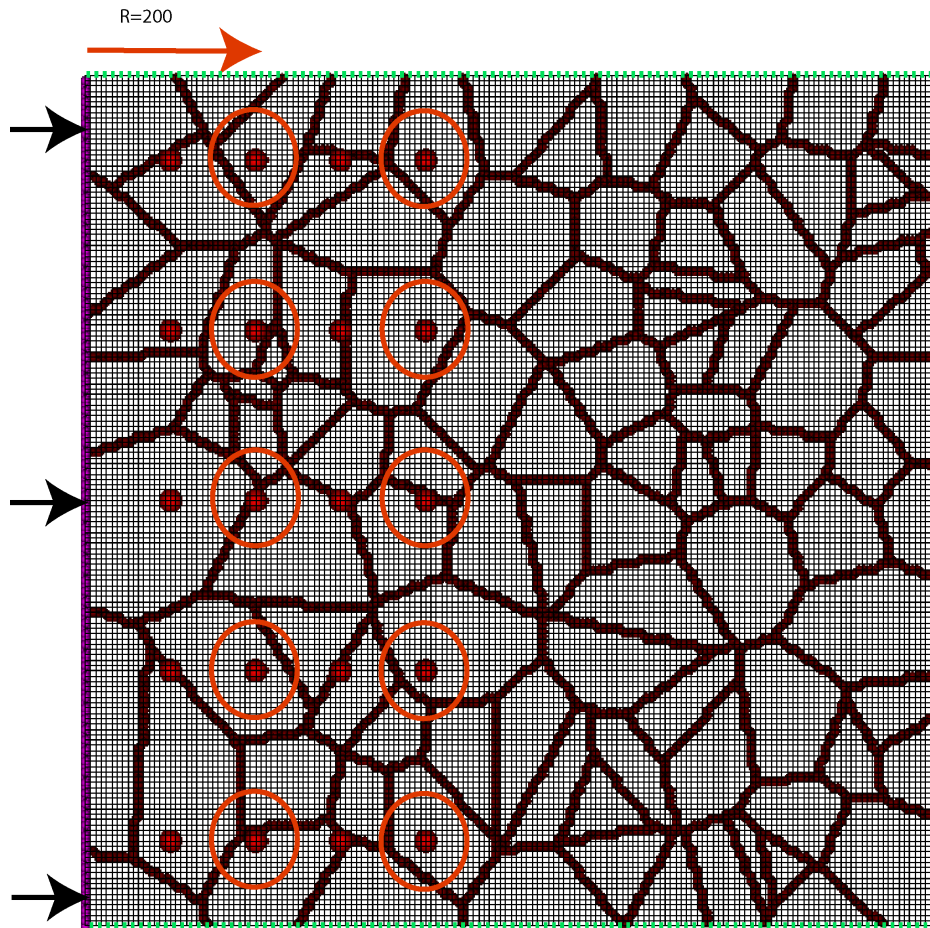


Figure 18. Computational mesh, boundary conditions and the location of the representative volumes for dynamic uniaxial loading of 100 blocks using velocity boundary on the left.

The axial stress in discrete simulations stays constant as well as the velocity and is proportional to the velocity value with the coefficient of proportionality being the effective impedance of the system. It is seen from comparing Fig.19 and Fig.20 that the impedance is reduced when the number of joints is increased. Also, the rate of the deviatoric stress relaxation seems to increase with increased number of joints. Figure 21 shows trajectories in stress-pressure space recorded in RVs during the plane wave loading at two different velocities 200 m/s and 100 m/s for the assembly of 1000 blocks. It is seen from the picture that, unlike in quasi-static loading, in the dynamic loading the deviatoric stress drops after reaching its peak due to the stress relaxation (shown with arrows). Note, that the rate-dependent aspects of the intact model were not exercised in these calculations and that the intact model was assumed to be strain-rate independent. Also, we have disabled the strain softening but still observed the stress relaxation effect.

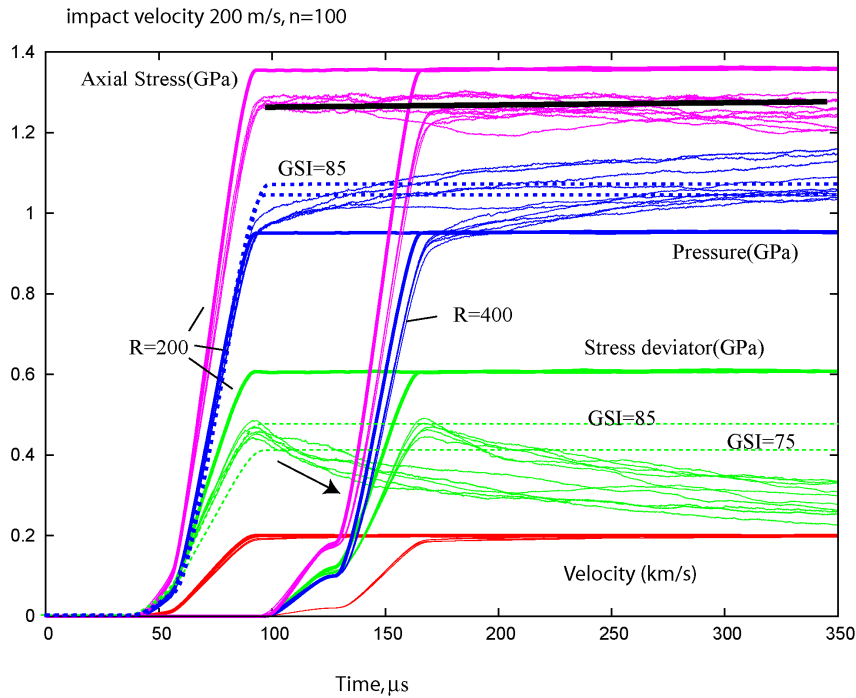


Figure 19. Evolution of the stresses and velocity in RVs at two ranges ( $R=200,400$ ) in a plane strain loading for 100 blocks. Deviatoric stress relaxation at RVs (5 at each location) is shown with the arrow. The bold solid lines correspond to the intact material, the dotted lines correspond to the continuum calculations with intact material with reduced strength properties.

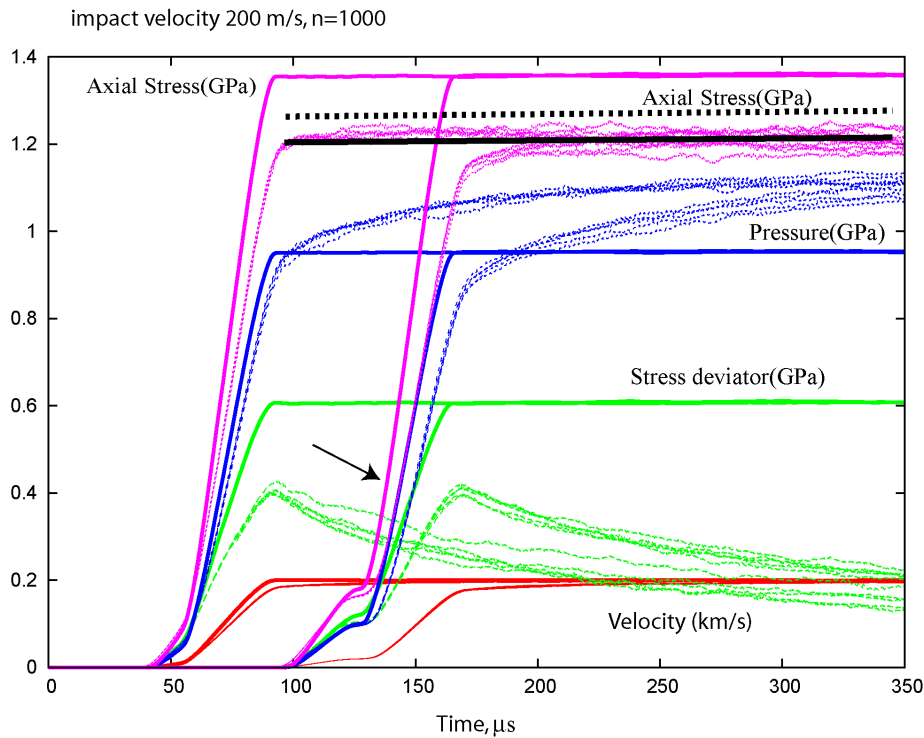


Figure 20. Evolution of the stresses and velocity in RVs at two ranges ( $R=200,400$ ) in a plane strain loading for 1000 blocks. Deviatoric stress relaxation is shown with the arrow. The bold dashed line shows the stress level achieved for 100 blocks.

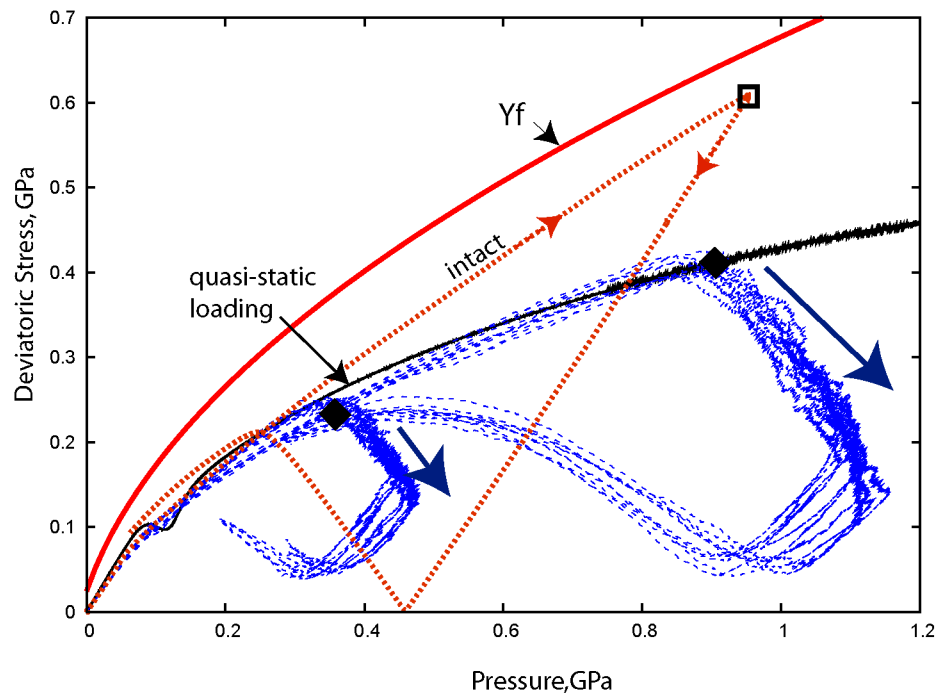


Figure 21. Loading trajectories in Y-P plane for intact rock reaching the states behind the plastic wave shown with markers (square for the intact material and diamond for the jointed material with 1000 blocks).

### Dynamic in-Situ homogenization

One reason the adequate EC model is difficult to build is that the representative volume elements are often tested for simple loading conditions such as uniaxial strain or simple shear. In reality, material can be subject to much more complicated loading conditions. We suggest in the current approach to record loading histories in Situ during the high fidelity calculations with explicit joint representation together with the mechanical response history of the representative volumes. The next step is to apply the recorded loading history to a single continuum element and tune the model parameters to match the response. Thus, instead of doing iterations running the large problem with the equivalent continuum and trying to modify the model to match the results of the high fidelity model, the EC model can be built using a material driver if the target response is known and only then be validated in large scale calculations.

We considered a problem of a cylindrical wave propagation generated by an instantaneous energy deposition as shown in Fig.22. The source was modeled using a circular region filled with an ideal gas with density 2.7 g/cc and buried 100 mm under the surface. The wave generated by the source was propagating down to the cavity of radius 50mm located 700 mm below the surface. The goal of this study was to find an equivalent continuum model which would produce very similar loading on the cavity. Fig.23A-23B shows pressure contours calculated for two different joint densities. When intact continuum model was used (Fig.23C), the wave formed propagated with a higher velocity and consisted of a distinct elastic precursor followed by the plastic wave. The equivalent continuum models EC1 and

EC2 build for this uniaxial dynamic loading-unloading regimes produced better results shown. Figure 24 shows the pressure contours calculated with one of these EC models (EC2). Elastic precursor has been reduced and the pressure level was increased in the wave which agrees better with the discrete simulation results shown in Fig.23B. Figure 24 compares radial velocity evolution at location B3 above the cavity found in discrete and continuum calculations.

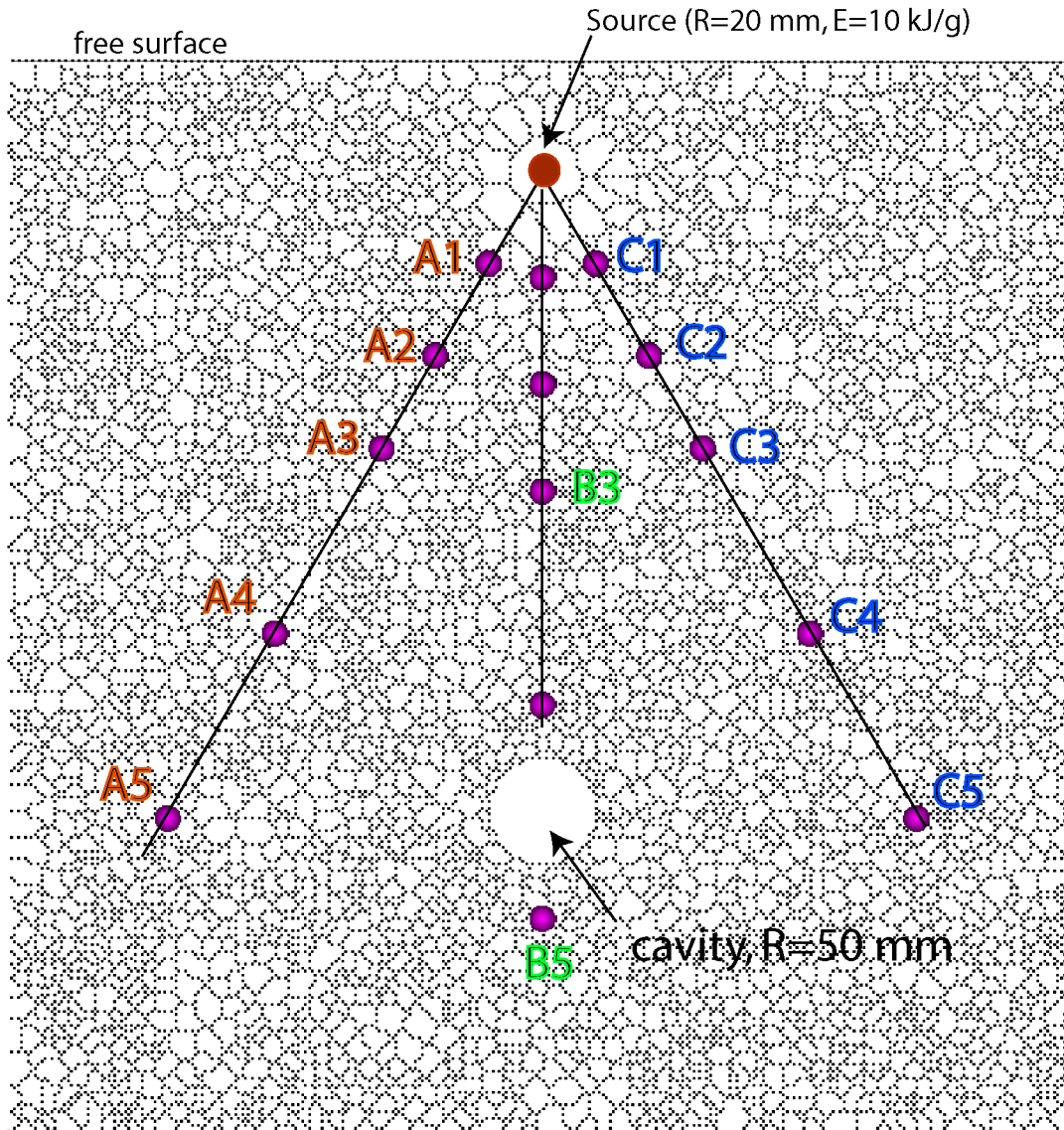


Figure 22. Block boundaries and RV point locations for 4000 block. The size of the region is 1000x1000 mm.

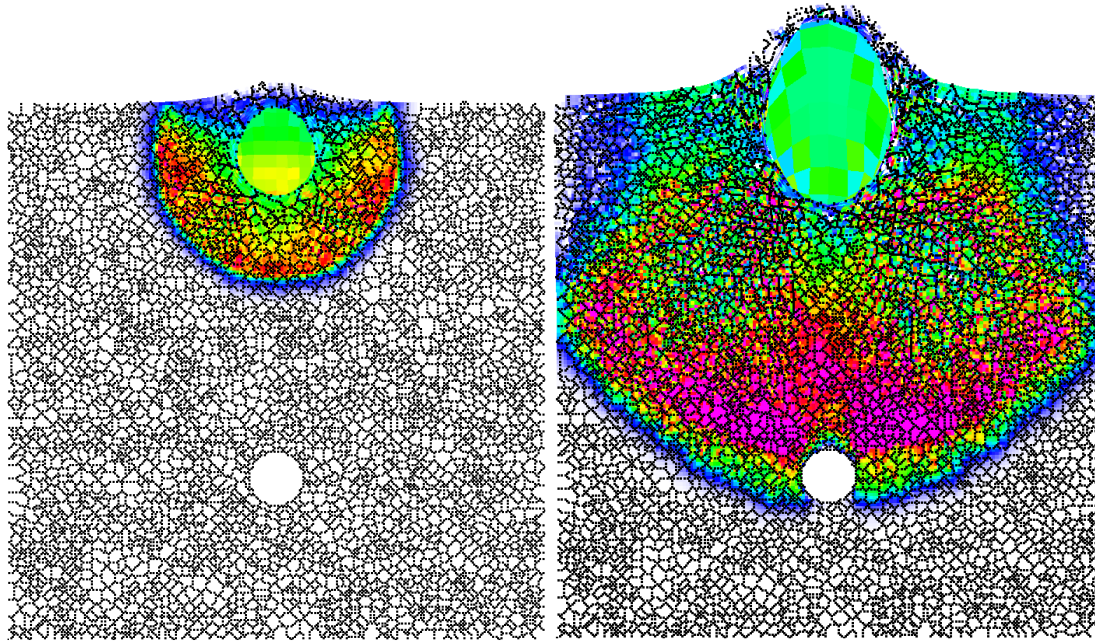


Figure 23A. Pressure contours at 100 ms (0-0.5 GPa) and 300 ms (0-0.1 GPa) for 4000 blocks. Friction angle = 11, the joint stiffness is 1 GPa and the joint aperture 1 mm.

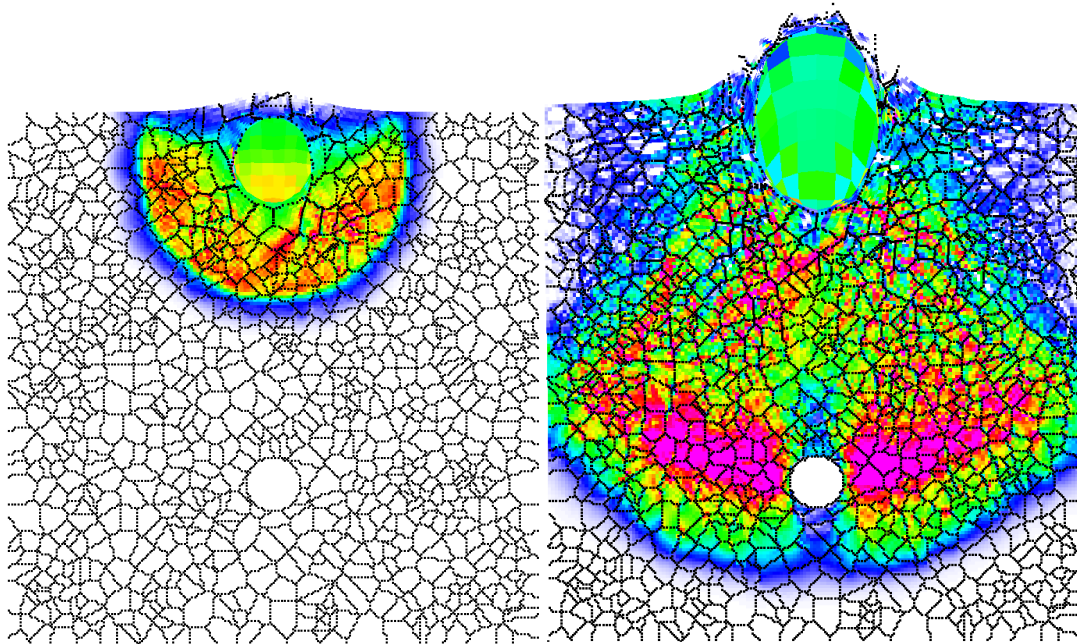


Figure 23B. Pressure contours at 100 ms (0-0.5 GPa) and 300 ms (0-0.1 GPa) for 1000 blocks. Friction angle = 11, the joint stiffness is 1 GPa and the joint aperture 1 mm.

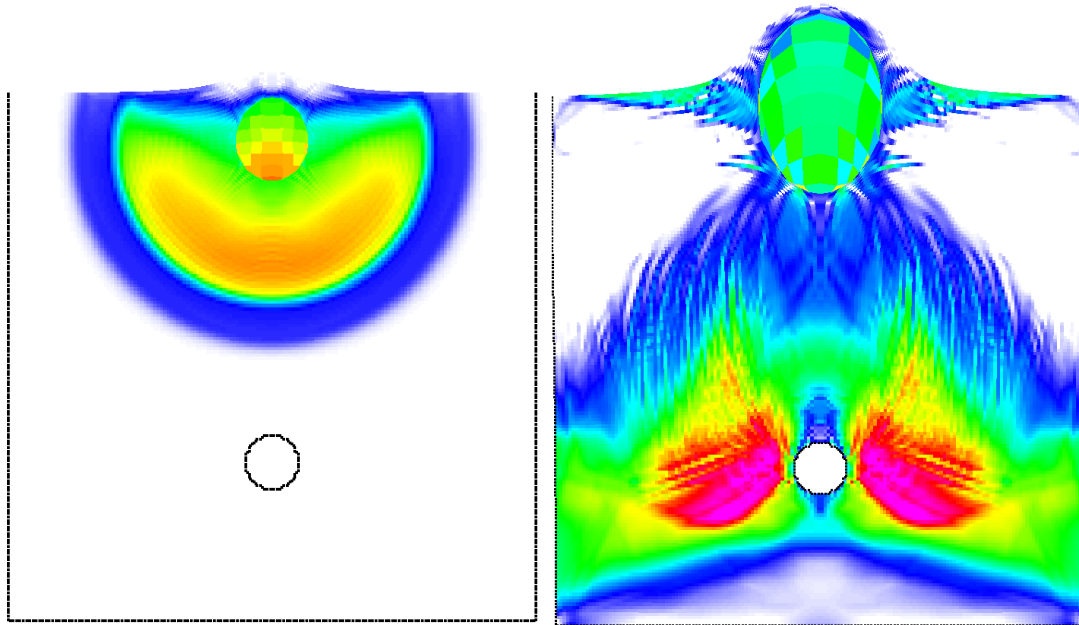


Figure 23C. Pressure contours at 100 ms (0-0.5 GPa) and 300 ms (0-0.1 GPa) for intact material.

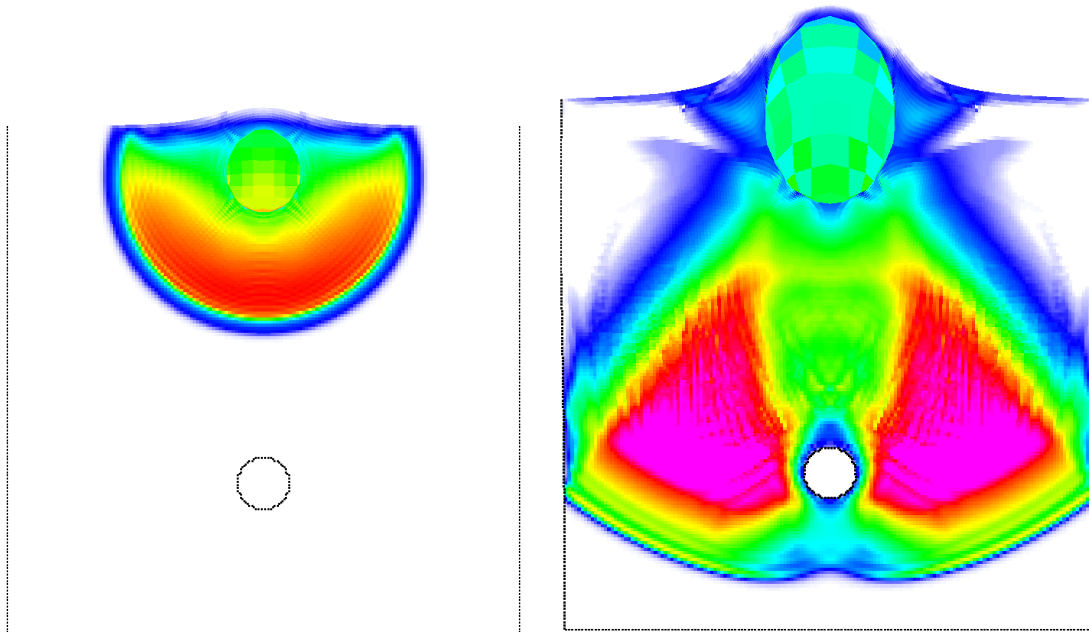


Figure 23D. Pressure contours at time=100 micsec (0-0.5 GPa) and 300 ms (0-0.1 GPa) for equivalent continuum model with reduced strength and modified compaction parameters.

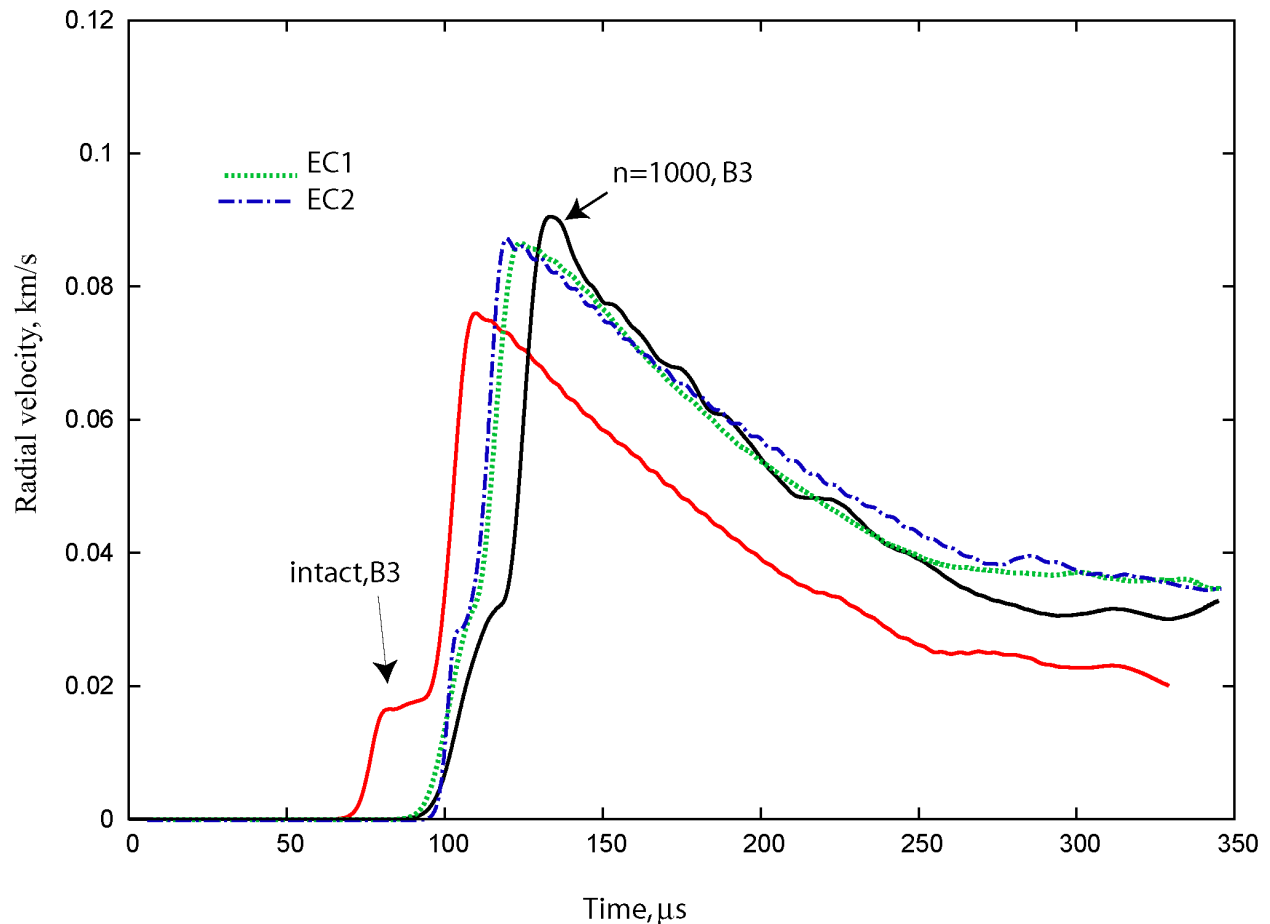


Figure 24. Radial velocity evolution at location B3 for intact and jointed ( $n=1000$ ) material. Dashed lines correspond to EC model calculations.

## COMPUTATIONAL STRATEGIES FOR NUMERICAL SIMULATIONS OF WAVE PROPAGATION THROUGH JOINTED MEDIA

Accounting for every single joint in the problem may not be possible, therefore Equivalent continuum modeling should be used. But there will be regions in the problems where EC model may not perform very well. Figure 25 below shows schematically how such regions can be calculated in a large problem using discrete methods available in DEM codes or in FE codes with robust auto-contact capabilities. Equivalent continuum model can be built using the *dynamic in-situ homogenization* technique described above by solving large scale problem once using discrete models wherever possible and recording the loading conditions and the average mechanical response in Representative volumes located in areas of interest. Then using the recorded information an equivalent continuum model can be built which is designed for the particular problem and thus has better chances to adequately describe mechanical response of the jointed rock mass. Such an approach should help to understand how to build equivalent continuum models for a particular class of problems. We have shown that the transition from the static model to the dynamic model may not be trivial, which is another reason to use an in-situ homogenization technique.

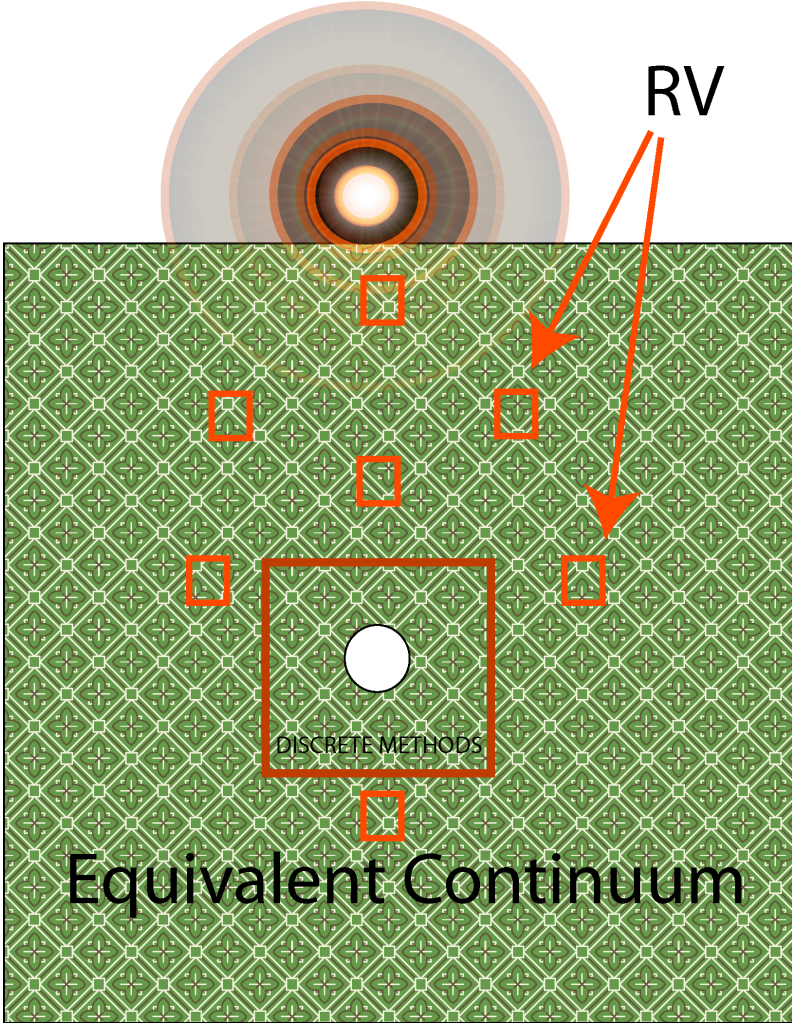


Figure 25. Schematic representation of combined discrete continuum computational strategy.

## CONCLUSIONS

- We have developed nonlinear models both for intact rock materials and joints capable of reproducing mechanical response observed in experiments on static and dynamic loading intact rock samples and joints.
- Combined mechanical response has been studied in numerical simulations where the joints were modeled explicitly using an advanced contact algorithm developed in the GEODYN-L code [11]. The study revealed that the overall mechanical response is strongly nonlinear and depends both on both material and joint properties. When the joints have a preferred orientation the response is anisotropic and when the joints are distributed randomly the response is isotropic.
- The study shows that, when the joints are confined, their effect on wave propagation is minimal. As the pressure level drops (due to attenuation or incoming release waves) the effect of joints becomes important. The introduction of joints tend to weaken the rock mass but this weakening is not uniform as some scaling rules used in geomechanics (for example, GSI based Hoek-Brown scaling rule) suggest.
- We have conducted a comparison between explicitly modeled jointed media and a weakened homogenous rock material to find out to what extent uniformly weakened isotropic material can reproduce the response of the jointed rock. Results of simulations indicate that we need an anisotropic plasticity model to reproduce the response of the jointed rock with just two sets of joints. Better results can be obtained if the joints are oriented randomly.
- We have considered a natural way of building a homogenized continuum for a randomly jointed media by loading a Representative Volume quasi-statically and fitting a homogeneous model by matching its response. This technique was used in our previous studies to derive a homogeneous model by doing a triaxial-test on the RV and deriving an equivalent response [6]. We found that, for dynamic problems, the equivalent homogeneous model derived in quasi-static tests may not be as good. We conducted a study of plane waves propagating through a jointed medium which showed that the deviatoric stress is not constant behind the plastic front as it would be if any homogeneous model were used. This relaxation is related to the multiple elastic waves running between the joints and the boundaries, which shift the equilibrium between the volumetric and deviatoric compressions.
- Considering that it is very difficult to build an EC model that reproduces all features of a discrete model (for example, dynamic relaxation found in this study), and also the fact that the loading path can be different in different problems, we have suggested a better way of doing homogenization for the dynamic problems, *dynamic in-situ homogenization*. The essence of this approach is to record the loading history (velocity gradient evolution) for a few representative volume sets in the locations of interest, as well as the mechanical response in these volumes (the stress state and some history variables such as the average damage, porosity and plastic strain). The homogenized model is then built by exercising the material driver to optimize the parameters in the homogenized model to match the recorded responses.
- In the end we suggest to use a hybrid computational approach as a strategy for efficient calculations of large scale problems with multiple joints. The essence of this approach is to use discrete joint representation only in the areas where it is absolutely needed and replacing the jointed medium with the equivalent continuum where possible.

## REFERENCES

1. Vorobiev O, Liu B, Lomov I, Antoun T. Simulation of penetration into porous geologic media. *International Journal of Impact Engineering* 2007; 34(4):721 – 731
2. Hoek, E., Brown, E.T., 1998. Empirical Strength Criterion for Rock Masses, *Journal of the Geotechnical Engineering Division, American Society of Civil Engineers* 106(GT9), 1013-1035
3. Bandis, S.C., Lumsden, A.C., Barton, N.R., 1983. Fundamentals of Rock Joint Deformation. *Int. J. Rock. Mech. Min. Sci. Geomech. Abstr.* 20(6),249-268
4. A. Fossum, Effective elastic properties for a randomly jointed rock mass, *Int.J.Rock mech.min.sciences Geomechanics Abstracts*, 1985,22(6),pp.467-470
5. M. Cai and H.Horii, A constitutive model of highly jointed rock masses, *Mechanics of Materials*,1992,13,pp.217-246
6. Ki-Bok Min and L. Jing, Numerical determination of the equivalent elastic compliance tensor for fractured rock masses using the distinct element method, *Int.Journal Rock Mech& Mining Sciences*, 2003, 40,pp.795-816
7. K.Terada,M.Hori,T.Kyoya,N.Kikuchi, Simulation of the multi-scale convergence in computational homogenization approaches, *Int.J.Solids and Struc.*, 2000,37, pp.228502311
8. V.G Kouznetsova, M.G.D Geers, W.A.M Brekelmans, "Multi-scale second-order computational homogenization of multi-phase materials: a nested finite element solution strategy, *Comput.Methods Appl.Mech.Engng.* , 2004,193, pp.5525-5550
9. O.Vorobiev Generic strength model for dry jointed rock masses, *Int.Journal of Plast.*,2008,24(12,pp.2221-2247
10. O. Vorobiev, Discrete and continuum methods for numerical simulations of nonlinear wave propagation in discontinuous media, accepted in *International Journal for Numerical Methods in Eng.*, 2009
11. O.Vorobiev, Simple Common Plane contact algorithm for explicit FE/FD methods, submitted to *Comput.Meth.Appl.Mech.Engng*, 2009
12. G.Exadaktylos and M. Stavropoulou, A specific upscaling theory of rock mass parameters exhibiting special variability:Analytical relations and computational scheme, *Int.Journal Rock Mech& Mining Sciences*, 2008, 45,pp.1102-1125
13. A.Pouya and M.Ghoreychi, Determination of rock mass strength properties by homogenization, *Int.J.Num.Anal.Meth in Geomechanics*, 2001,25, pp.1285-1303
14. Gefken P, Florence A. Spherical waves in jointed limestone. Technical Report DNA-TR-92-122, SRI 1993
15. Vorobiev OY, Antoun TH, Lomov IN, Glenn LA. A strength and damage model for rock under dynamic loading. *AIP*, 2000; 317–320

**This work performed under the auspices of the U.S. Department of Energy by Lawrence Livermore National Laboratory under Contract DE-AC52-07NA27344.**